Physics – Uspekhi **58** (10) 933 – 951 (2015)

REVIEWS OF TOPICAL PROBLEMS PACS numbers: 73.63.Rt, **75.75. – c**, 81.07.Lk

Formation and properties of metallic atomic contacts

A L Klavsyuk, A M Saletsky

DOI: 10.3367/UFNe.0185.201510a.1009

Contents

Abstract. One of the most topical and promising areas in present-day physics is the study of the physical properties of metallic few-atom contacts, which are attractive not only for their application prospects, but also because of the possibility to verify with their aid various theoretical approaches through theory-vs-experiment comparison. This review mainly focuses on theoretical approaches to understanding the formation processes and properties of metallic atomic contacts.

Keywords: metallic nanowires, metallic nanocontacts, quantum conductance, nanomagnetism, spintronics

1. Introduction

One-dimensional metallic structures have recently become an object of extensive research, because they provide a promising nano-scale material for manufacturers of electronic components hoping to utilize them for the further miniaturization of their products. One-dimensional atomic nanostructures on the metal surfaces may be instrumental in promoting technological advances in electronics and other sectors [1–3]. Therefore, a priority task now consists in creating metallic one-dimensional atomic structures with controllable properties.

By one-dimensional atomic structures on a metal surface are meant atomic contacts (an atom or a chain of several atoms connecting two macroscopic electrodes) and nanochains (linear chains of atoms on a metal surface).

The present review is confined to the description of the properties of metallic atomic contacts. Why exactly metallic? We hope that our review will just give the reader an answer to this question. Briefly, metallic contacts are especially attractive for at least two reasons. First, nanocontacts connecting two electrodes exist in a free space. The properties of long atomic contacts, similar to those of surface clusters, are only weakly influenced by the surface, which makes them attractive in terms of the possibility to compare the theoretical and experimental data yet obtained. Second, such nanocontacts connect two metal electrodes and therefore can be used for direct measurement of their electrical properties.

The creation of atomic contacts in an experiment was first reported in Ref. [4], where gold atomic contacts with conductance equal to conductance quantum $G_0 = 2e^2/h$ were obtained and existed for a few minutes at a low temperature. The quantum behavior of conductance had also been demonstrated in earlier studies [5–9], but the authors of Ref. [4] not only reached a minimal conductance of $(12.9\ \mathrm{k\Omega})^{-1}$ for nanocontacts but were the first as well to propose an experimental method for elucidating their atomic structure. The possibility of forming atomic contacts more than one atom in length opened up new prospects in both

A L Klavsyuk, A M Saletsky Faculty of Physics,
Lomonosov Moscow State University,
Leninskie gory, 119991 Moscow, Russian Federation
E-mail: klavsyuk@physics.msu.ru, sam@physics.msu.ru

Received 23 June 2015, revised 15 July 2015
Uspekhi Fizicheskikh Nauk **185** (10) 1009 – 1030 (2015)
DOI: 10.3367/UFNr.0185.201510a.1009
Translated by Yu V Morozov; edited by A Radzig

basic and applied physics. Before that, the structure of atomic contacts had been determined by comparing experimental conductance histograms and theoretical findings.

At present, the properties of atomic contacts are investigated by scanning tunneling microscopy (STM) [7, 10, 11], the mechanically controllable break junction (MCBJ) technique [12–15], high-resolution transmission electron microscopy (TEM) [4, 16–19], and atomic force microscopy (AFM) [11, 20]. Sometimes, a combination of these experimental methods is applied for simultaneous investigation of, say, the structure and conductance [4] or mechanical properties [21]. In most cases, however, different types of microscopes are employed individually for technical reasons.

As far as theoretical approaches to the study of atomic contact properties are concerned, most of them are based on *ab initio* calculations or molecular dynamics (MD) simulation [22–28]. The kinetic Monte Carlo method (KMCM) has found application only in recent work for the study of atomic contact formation [29, 30].

It should be mentioned for readers unfamiliar with the research area in question that atomic contacts were shown to possess unique physical properties, such as ballistic quantum conductance, ballistic magnetic resistance, and giant magnetic anisotropy. Moreover, atomic contacts, like other low-dimensional structures, are very strong. In this review, we describe the most characteristic properties (mechanical, electronic, magnetic) of one-dimensional quantum structures and discuss the peculiarities of their formation. Also, we shall try to analyze and evaluate the advantages and disadvantages of different theoretical approaches to the investigation of nanocontact properties based on a comparison of available theoretical and experimental data.

2. Formation of atomic contacts

2.1 Experimental methods for the creation of atomic contacts

Currently, STM, AFM, TEM, and the mechanically controllable break junction technique are the most extensively used methods for the formation of atomic contacts. Let us consider them in more detail.

STM and AFM are actually employed as powerful universal tools for obtaining a deeper insight into nanostructure properties and formation. Specially prepared needles are used in scanning microscopes, the characteristic distance between the tip of the needle and the surface under study being 0.1–10 nm. In a normal scanning regime, the needle surveys the surface without forming atomic contacts. Two scanning regimes are feasible: the constant tunneling current mode, and the constant average distance mode. However, the tip–sample spacing is so small that surface scanning sometimes gives rise to atomic contact. This feature of scanning microscopes suggests the possibility of their application not only for structural research at the atomic level but also for the formation of new structures.

Specifically, STM was exploited for creating linear atomic contacts [4, 31]. To this end, the miniature needle of the scanning microscope was dipped into a gold cluster and moved slowly under the control of an electron microscope. The movement of the needle caused gradual reduction of the nanocontact width (Fig. 1a). Its break was preceded by the formation of a linear atomic chain connecting two electrodes (Fig. 1a). It took a few seconds to form a linear atomic chain

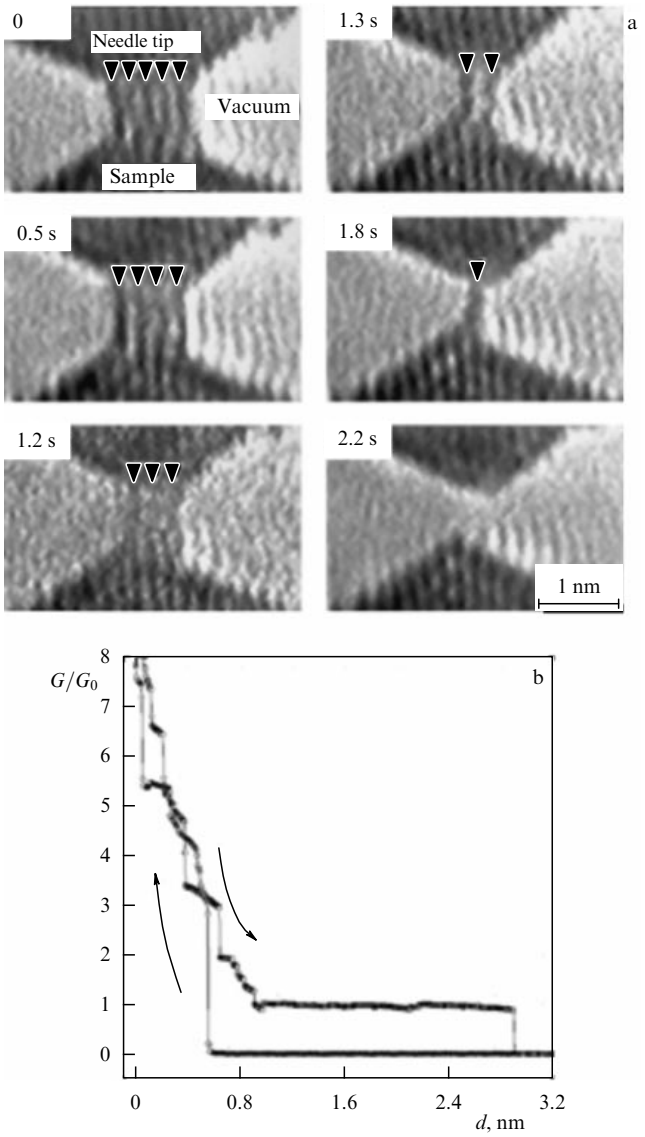

Figure 1. Formation and conductance of gold nanocontacts. (a) The structure of a gold nanocontact upon stretching for different time intervals (0–2.2 s). The nanocontact is formed between the STM needle (top) and the gold surface (bottom) [4]. (b) Relative conductance G/G_0 as a function of displacement d of two electrodes during atomic contact formation at 4.2 K [12].

sometimes composed of up to 10 atoms [31]. The use of STM made it possible to form atomic contacts both at low and room temperatures.

It should be noted that the stretching of metallic contacts results in a discrete reduction of conductance by $2e^2/h$, as follows from the graph of relative conductance for a gold nanocontact (Fig. 1b). The length of the plateau with conductance $2e^2/h$ at low temperatures (Fig. 1b) is roughly 2 nm. These two characteristic features give evidence that, first, a linear atomic contact is formed and, second, it is rather stable at low temperatures and therefore amenable to further stretching.

Another method for the formation of metallic atomic contacts is the so-called mechanically controllable break junction technique. In this method, a notched thin wire of the sample metal (some 0.1 mm in diameter) fixed on a substrate is bent with a piezoelement till it breaks. The

experiment is carried out in a vacuum at a low temperature, which not only prolongs the lifetime of the nanocontact but also guarantees the absence of impurities. The method allows atomic contacts to be formed and their properties, e.g., conductance, to be investigated [12–15]. Its sole disadvantage lies in the fact that it does not permit the atomic structure to be visualized.

TEM is currently the only method suitable for application in nanocontact technologies. With this method, an electron beam is used to burn two nearby holes in a thin metal film with a narrow (1–2 nm) passage between them. The passage then breaks down as a result of self-organization of atomic positions in the absence of any external impact [16]. Video images of the process are analyzed after it terminates. The contact created by TEM does not elongate. Thinning of the contact is due exclusively to atomic diffusion inside it [29, 30, 32]. TEM makes it possible to form atomic contacts from practically all 3d-, 4d-, and 5d-metals at room temperature. By way of example, nanocontacts have been formed from Co [33], Cu [34, 35], Rh [36], Pd [33], Ag [37], Pt [32, 33], and Au [38, 39] and their properties investigated.

2.2 Simulation of the atomic contact formation by the molecular dynamics method

With recent progress in computing technology, simulation has become a most important research tool in modern physics. In scattered instances, simulation is the sole method allowing the answer to certain questions to be obtained, which accounts for one of its main advantages over experiment. Simulation of atomic contact formation in Refs [22, 23] showed that elongation of a nanocontact is associated with the breaking of atomic bonds inside it. The contacts themselves are formed from surface atoms.

One of the simplest and most frequently applied methods for simulation of nanocontact formation is the molecular dynamics method. The following protocol is usually used to simulate dynamic stretching of nanocontacts: atomic contacts composed of several atoms are positioned between two electrodes, each having a few fixed layers (in other words, a contact is placed between two bulk crystals). All atoms initially occupy the crystal lattice sites. If a metal has the face-centered cubic (fcc) crystal lattice, an almost circular cross section of the nanocontact is chosen as energetically preferred for such contacts. The nanocontact is stretched by altering the spacing between the two electrodes in a stepwise fashion. Both the step and the time are determined by the chosen stretching speed. If stretching occurs at a given temperature, a proper thermostat is needed to maintain it at the desired level.

When running the molecular dynamics method, special care should be taken to choose the potentials [24] describing interatomic interactions. Figure 2a–c presents the structures of a gold nanocontact at room temperature obtained with the selection of three different semiempirical potentials, viz. the Cleri–Rosato potential [40], glue model potential [41], and embedded atom method potential [42]. The figure demonstrates that the structure of the nanocontact being stretched depends on the choice of the potential. The criterion for the correct choice of potentials for the study of the properties of metallic nanocontacts is agreement between the contact configuration energy and the energy calculated in the framework of the density functional theory.

The influence of the choice of potentials on the gold nanocontact structure is illustrated by Fig. 2d, which

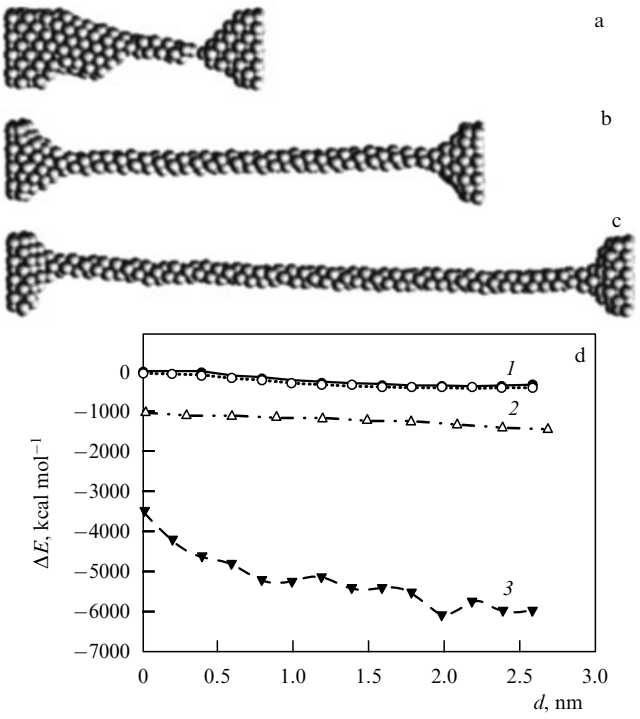

Figure 2. Structure of an Au(001) nanocontact upon stretching with the use of the (a) Cleri–Rosato potential, (b) glue model potential, and (c) embedded atom method potential. (d) Energy variation upon nanocontact stretching versus results of *ab initio* calculations for three potentials: Cleri–Rosato (curve *1*), embedded atom method (curve *2*), and glue model (curve *3*) [24].

compares energies obtained with the use of the Cleri–Rosato (curve *1*), embedded atom method (curve *2*), and glue model (curve *3*) potentials. The energy values calculated by the pseudopotential method in the framework of the density functional theory [24] are taken to be zero. The data presented in the figure indicate that the Cleri–Rosato potential is the best choice for simulating the formation of gold nanocrystals, even though the use of the embedded atom method potential also yields a good result, unlike the glue model potential [24]. Moreover, simulation of nanocontact formation implies taking into consideration that its stretching rate in experiment is 10^{-8} m s^{-1} or much lower than in the MD method (10^{-2} m s^{-1}). Disregarding this fact does not allow taking into account diffusion processes in the system. Atomic diffusion in metallic nanocontacts is practically absent at low temperatures, and the results obtained by the MD method are then in excellent agreement with experimental data.

The direction of nanocontact stretching is of importance for the formation of an atomic chain. It was shown in experiment that direction [110] is the preferred orientation for the formation of atomic contacts at low temperatures by the mechanically controllable break junction technique [4, 37]. The advantage of stretching in the [110] direction over that in the [100] and [111] directions is due to the fact that atoms of the nanocontact in the [110] case are less densely packed, which enables them to extend to a greater length due to the smaller number of bonds that need to be broken [43]. Moreover, the surface energies for the (110) direction in many 3d-, 4d-, and 5d-metals are higher than for (100) and (111) [44]; therefore, it is more difficult for a nanocontact

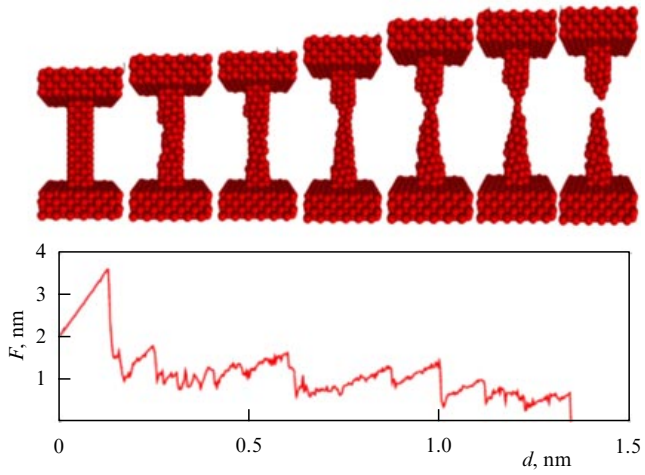

Figure 3. Dependence of the structure and elastic force F emerged in a wide gold contact stretched along the [100] direction on the distance between electrodes [26].

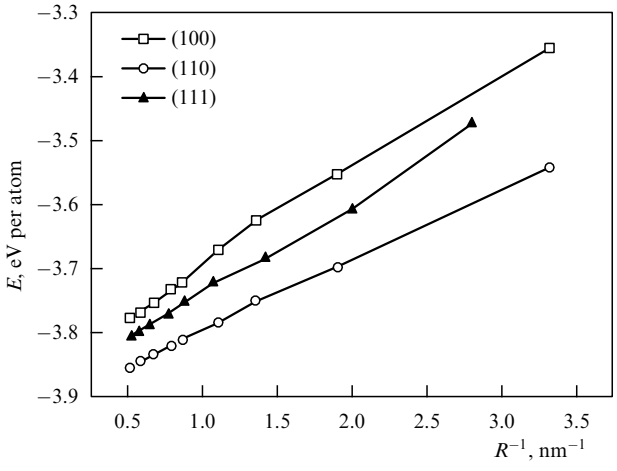

Figure 4. Mean potential energy per atom as a function of the inverse of the palladium nanocontact radius for (100), (110), and (111) orientations of electrode surfaces [47].

stretched in the [110] direction to maintain its structure than for nanocontacts stretched in the [100] and [111] directions.

Stretching nanocontacts is accompanied by their structural changes [25–27]. By way of example, Fig. 3 presents the dependence of the elastic force on the distance between electrodes for a gold nanocontact with a diameter of 6 Å composed of several hundred atoms [26]. Prior to stretching, the contact had the fcc structure. The dependence of the elastic force on the distance between electrodes is of an oscillatory character (see Fig. 3). The elastic force first grows linearly upon stretching and sharply decreases thereafter, as in the case of an atomic contact [27], which, however, does not lead to the breakdown. It increases again upon further stretching but finally falls down. Such oscillatory behavior of the elastic force depending on the extent of stretching d is observed until d reaches the value corresponding to the break; it is related to structural changes in the contact being stretched. The linear increase in the elastic force depending on d corresponds to the elastic phase of stretching; in this case, the contact has the fcc structure. Further stretching gives rise to the inelastic phase associated with the formation of a disordered structure and a sharp decrease in the elastic force.

Thus, the process of contact stretching consists of a sequence of elastic and inelastic phases. Notice that contacts stretched in different directions [100], [110], [111] exhibit different behaviors [27, 28, 39, 45, 46]. Calculations for different metals, such as palladium [27], copper [28], and gold [39, 45], show that the [110] direction turns out to be especially 'flowable' because the number of elastic force jumps (phase changes) for the [110] direction is greater than for the [100], [111] directions. For this reason, the inelastic phase predominates in this case.

The probability of formation of atomic contacts prior to atomic chain breaking strongly depends not only on their chemical composition but also on the direction of stretching. Let us consider first the formation of nanocontacts at low temperatures when atomic diffusion is practically absent. In this case, a change in contact properties needs to be taken into account due to diminishing of the contact diameter upon stretching. This situation is exemplified by a palladium nanocontact [47].

Figure 4 shows the dependence of the potential energy per atom on the inverse of the nanocontact radius. All three straight lines must intersect at a common point corresponding to the binding energy in a perfect crystal, while the angles of their slope depend on the surface energy of the facets making up the palladium nanocontact [48]. It follows from Fig. 4 that the mean potential energy per atom, when the nanocontact is located between two electrode surfaces oriented in the (110) direction, is minimal for all lateral sizes of the nanocontact. Therefore, stretching may cause spontaneous structural rearrangement of the contact having a finite radius and located between electrode surfaces oriented in a direction other than (110); such a rearrangement will most likely lead to its breakdown. On the one hand, palladium nanocontacts placed between electrode surfaces oriented in the (110) direction feature the highest stability upon stretching; on the other hand, they are at the highest risk of breakdown without formation of atomic contacts. The energy is higher for other orientations of the electrode surfaces, and the potential barrier for the formation of atomic contacts is lower. This means that temperature must be such that it enables the system to overcome the barrier without breaking the nanocontact.

Of no small importance is information on those metals in which atomic contact form and in which they are not. A variety of parameters are used to identify metals more or less suitable for the formation of atomic contacts. The authors of Ref. [49] proposed using the ratio of the breaking force for an infinite chain to the bond breaking force in a crystal as such an estimation parameter. In a later study [47], the ratio of the atomic binding energy in a one-dimensional chain to that in a crystal was used as the criterion for the formation of atomic contacts. Both criteria show how strong the bonding is in one-dimensional structures compared with that in a perfect crystal. Thus, the higher the estimation parameter, the greater the probability of formation of linear atomic contacts. The propriety of the application of these parameters was confirmed both in experiment [50] and by computer simulations [47]. The sole difference is that the former parameter fails to account for the high probability of formation of palladium atomic contacts. Moreover, the latter parameter is simpler to calculate, because the computa-

Table 1. Breaking force values (in nN) for metallic atomic contacts with electrode surface orientation in the (100), (110), and (111) directions for an infinite chain and a perfect crystal.

Metal		(100)	(110)	(111)	Chain	Crystal
Cu	[35, 47]	1.1	1.2	1.3	1.4	0.5
Rh	[47]	1.6	1.6	1.5	1.9	1.1
Pd	[47]	1.7	1.6	1.9	1.2	0.6
Ag	[47, 51]	1.0	1.1	1.2	1.3	0.5
Pt	[47]	2.6	2.5	2.9	2.6	0.9
Au	[24, 25, 39, 45]	1.5	2.2	1.6	2.1	0.7

tion of the binding energy for nanocontacts is less laborious than the computation of their breaking force. According to these criteria, gold and such 5d-metals as iridium and platinum are much more suitable than silver and copper for the formation of linear atomic contacts at low temperatures [47, 49, 50].

It was mentioned in a preceding paragraph that diffusion processes at a low temperature can be disregarded, but the physics of atomic structure formation changes radically as it rises (see below). Notice that the atomic contacts of many metals, including 3d- and 4d-ones, are known to form at room temperature [33–35]. Therefore, we shall discuss here only the formation of atomic contacts immediately before breaking.

One of the parameters determining the probability of atomic contact formation is the breaking force. Calculations reveal that bond breaking forces of linear atomic contacts differ for different metals and depend on the orientation of electrode surfaces (Table 1) [24, 25, 35, 39, 45, 47, 51]. For example, a linear contact from copper atoms is especially strong between the electrodes oriented in the (111) direction and becomes very weak in the (100) orientation. The strength of linear atomic contacts in gold is minimal between electrode surfaces oriented in the (110) direction.

These observations are confirmed by the results of experiments at room temperature indicating that the probability of forming copper [35] and gold [39] linear atomic contacts depends on the orientation of the electrode surfaces. The preferred orientation for metals is that associated with the highest breaking force of linear atomic contacts. This fact can be explained as follows. Atomic diffusion at room temperature results in the rapid formation of a single-atom contact, with the metal near the contact having the same crystalline structure as the electrodes. Then, the nanocontact with the maximum breaking force provides the highest probability of forming a linear atomic contact upon further stretching, in excellent agreement with experiments [35, 39].

The probability of forming atomic contacts can be enhanced by introducing various impurities, such as oxygen [52] and hydrogen [53] molecules, that change the electronic properties of the nanocontacts [54] and thereby affect their atomic structure and other physical characteristics. The impurities can promote both destruction and stabilization, i.e., strengthening, of the nanocontact [52–54].

2.3 Simulation of the atomic contact formation by the kinetic Monte Carlo method

Ongoing theoretical studies of the formation of atomic contacts are mostly carried out by two methods: MD with the use of semiempirical potentials [27, 38, 47], and calculations in the framework of the density functional theory [45, 55]. Both techniques reduce to the simulation of a decrease in the cross section and a break of the nanocontact upon its elongation. However, a contact formed by TEM avoids elongation, and the cross section of the nanocontact decreases due to atomic diffusion alone. Moreover, it takes, as a rule, about 1 minute to form the nanocontact [16]. To simulate such a long process, some 10^{16} steps of the MD method need to be performed, which is impossible, in principle, at the modern level of computing technology. Thus far, the MD method has permitted simulating evolution of nanocontacts no longer than 20 fs in length [56].

Moreover, it was shown in experiment that conductance of nanocontacts strongly depends on the mode of their formation, i.e., either by stretching or self-organization [57]. The same factors determine the time of their existence. A nanocontact formed by stretching at room temperature was shown to exist for 0.01 s, in contrast to the lifetime of 15 s for a contact formed through self-organization. These observations suggest different mechanisms of formation of atomic contacts depending on the method by which they were obtained; hence, the necessity of an integrated approach to the formation simulation of atomic contacts.

It was proposed to address this issue by exploiting such a powerful tool for simulation of the formation of metallic nanocontacts as the kinetic Monte Carlo method (KMCM) [29, 30]. In so doing, the energy barriers for the main diffusion events were determined by the MD method. Such a combined approach to the investigation of surface atomic diffusion and self-organization of various nanostructures has recently found wide application for the study of both homogeneous and heterogeneous systems [58–60].

The process of nanocontact formation by TEM is arbitrarily divided into four steps [29, 30]. Let us consider them in more detail using a gold nanocontact as an example.

The narrow passage between two holes in the gold film immediately after their burning is an fcc crystal with (100), (110), and (111) facets that can have, in general, all possible edges between them. However, not all atomic positions in such a crystal are equivalent. Atoms located at the edges between (110) and (110), between (100) and (110), or between (100) and (100) facets have the lowest binding energy (3.53 eV, 3.54 eV, and 3.65 eV, respectively). Therefore, low-barrier events bearing the responsibility for the atomic transfer from these edges to crystal facets occur at the first stage of a nanocontact formation. Due to this, by the end of the first stage of nanocontact formation, the contact surface is made up of a combination of the (100), (110), and (111) facets arranged so that the aforementioned unstable edges are absent. Part of this contact surface is depicted schematically in the left part of Fig. 5a.

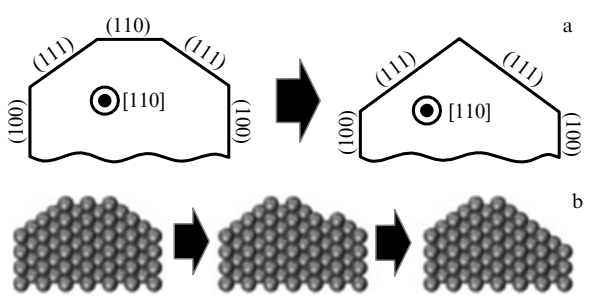

Figure 5. Schematic (a) and detailed (b) representation of part of a gold nanocontact in the course of its evolution. Part of the cross section normal to the [110] direction is shown [30].

At the second stage of nanocontact formation, the area of the (100) facets decreases, because they become energetically least favorable. This process (Fig. 5a) is related to the high mobility of gold atoms in the direction parallel to the edge between the facets, because the energy barrier for an atom jump, 0.32 eV, is much lower than other energy barriers. Moreover, it is energetically more advantageous for the atoms located at the edge to move to the (110) surface than to the (111) one. A gold atom must overcome an energy barrier of 0.70 eV to pass from the edge to a clear (110) surface, or a barrier of 0.65 eV if this surface is occupied by an atom. After this, the atoms move along the edge and leave the nanocontact region. If one or more atoms are already absent on the edge, it is easier for neighboring atoms to pass to the (110) surface. In the end, all atoms of a given edge leave the nanocontact region for 5×10^{-4} s; in this way, they free up a similar edge between the (111) and (110) facets. This process continues till all the atoms from the upper layer of the (111) surface leave the contact region, as shown in Fig 5b. Meanwhile, the area of the (110) and (100) facets decreases, while that of the densely packed surface (111) increases.

The second stage of nanocontact formation ends when the contact loses all (110) facets. At room temperature, this stage lasts about 1 s.

It is worthwhile to note that the direction of atom migration during the formation of atomic contacts is possible to control by an electric field. A recent experiment revealed that a nanocontact undergoes nonuniform deformation in the presence of an electric field [61]. The negatively charged electrode is slightly stretched, while the positive one is compressed; as a result, atoms migrate from the rarified region to the contracted one, i.e., toward the positively charged electrode.

The edges between (111) and (110) and between (111) and (111) facets in an fcc crystal are oriented in the [110] direction. If the narrow passage between the holes is initially oriented in the same direction, too, the self-organization leads to the formation of a nanowire, i.e., a nanocontact of uniform thickness. Any other orientation of the initial passage gives rise to a contact in the form of two 'pyramids' with overlapping vertices. This simulation-assisted prediction is consistent with experimental data for nanocontacts obtained at room temperature by TEM and other methods [9, 16, 32, 38].

At the third stage of nanocontact formation, they gradually become thinner as atoms move from the edges between (100) and (111) facets onto these facets. In the framework of the model being considered, such events prove impossible if the (100) and (111) facets have no defects, because the final state of the atom is unstable and it returns to the initial position. Therefore, thinning of the contact occurs either near its end or in the middle, where it is especially thin. The number of atoms capable of taking such jumps being much smaller than at the second stage, the third stage lasts an order of magnitude longer (around 1 minute). It ends in disintegration of the nanocontact crystal structure.

The fourth stage of nanocontact evolution occurs in the noncrystalline phase and continues till a single-atom nanocontact is formed. Disintegration of the crystal structure is accompanied by a manifold increase in the number of possible diffusion events. Also, it gives rise to low-barrier events leading to a rather rapid formation of a single-atom contact, which takes less time than thinning of a contact with the crystal structure.

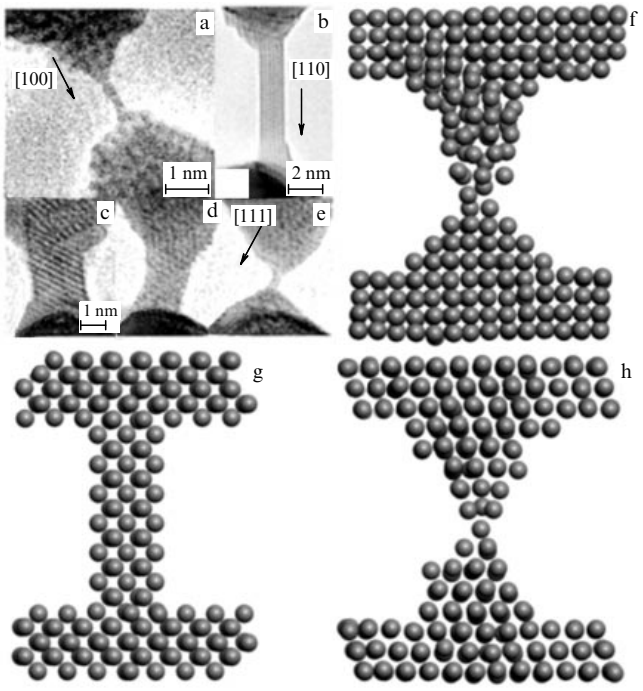

Figure 6. Formation of gold nanocontacts oriented along [100] (a, f), [110] (b, g), and [111] (c–e, h). Images of experimentally obtained nanocontacts (a–e) are borrowed from Ref. [16].

Figure 6 compares the results of computer simulations and an experimental study of the formation of gold nanocontacts. The best agreement between theory and experiment was achieved when the contact was oriented along the [110] direction (Fig. 6b, g). In this case, the nanowires being formed retain the crystal structure. If the contacts have the [100] (Fig. 6a, f) or [111] (Fig. 6e, h) orientation, an atomic contact is formed between the vertices of two pyramids. The crystal structure of contacts oriented in the [100] direction (Fig. 6f) undergoes much more pronounced disturbance than that of contacts oriented in the [111] direction (Fig. 6h). This result is also in excellent agreement with experiments [9, 16].

An analysis of the simulation of nanocontacts formed by the MD and KMCM methods gave evidence that formation by stretching and by hole burning in thin films is essentially different. In the former case, periodic alternation of crystalline and noncrystalline phases takes place, whereas in the latter case the noncrystalline phase occurs only at the end of evolution of the narrow passage. One more characteristic difference lies in the fact that the formation of atomic contacts simulated by the MD method involves surface atoms, whereas that simulated by KMCM recruits internal atoms. Thus, it is not always correct to compare experimental data obtained separately by TEM method and the mechanically controllable break junction technique.

3. Mechanical properties of nanocontacts

3.1 Nanocontact bonding length and geometry

It was mentioned in Section 2 that the break of a wide contact sometimes gives rise to an atomic contact. Detailed structural analysis showed that *prior to* the break atomic contacts can form by two independent mechanisms of nanocontact evolution [45]. In the first case, the elastic

phase transforms into the 'sliding phase' in which the atomic contact is stretched out and atoms lack strict ordering. In the second case, the elastic phase with its ordered atoms (as in a crystal) is followed by the 'defect formation phase' characterized by a regular crystalline organization of atoms and the appearance of defects due to bond breaking in the nanocontact upon its stretching. The nanocontact acquires a triangular cross section upon further stretching ('triangular phase'), which eventually gives rise either to a multiatomic contact or to the 'planar phase' in which atoms are arranged in two rows in the same plane. Sometimes, such structures are called *zig-zag* contacts [31, 55, 62–65]. The difference between zig-zag and planar contacts lies in the fact that all atoms in the former simultaneously build up linear atomic contacts during stretching. In the latter case, such contacts evolve as atoms gradually, one after another, gather into a linear structure in the course of stretching. The linear atomic contacts constitute metastable systems that undergo disintegration with time or when heated. Heating makes atoms of nanocontacts oscillate first only along the chain axis and thereafter in three directions, which gradually destroys the contact.

The zig-zag geometry of purely metallic nanocontacts awaits elucidation. *Ab initio* calculations suggest the possibility of emerging zig-zag geometry, but it is rarely observed in experiment, where it is attributed either to precession of one atom around the contact axis [65] or to the presence of an impurity that is difficult to resolve by an experimental technique [66, 67]. MD calculations revealed that the break of a zig-zag nanocontact occurs upon a small change in one of the two parameters, either temperature or the distance between the electrodes, because the energy barrier for the formation of the energetically advantageous zig-zag configuration of atomic contacts is higher than the energy needed to break it [68].

Structural analysis of atomic contacts evidenced two peculiar features, one being different interatomic distances in a contact and an ideal crystal, the other the nonuniform bond length distribution in atomic contacts [69]. As the number of atoms in a contact increases, the bond length distribution in the contacts becomes more uniform and the lengths themselves approach those in an infinite atomic chain.

Surprisingly, the interatomic distances in a contact can be much longer than in a crystal. For example, the atom–atom distance in gold contacts may be as large as 4.0 Å, compared with only 2.9 Å in a crystal (Table 2) [4, 21, 31, 37, 50, 51, 63, 68–74]. However, such a difference is not inherent in all metals (see Table 2).

Table 2. Experimental (a_{exp}) and theoretical (a_{calc}) bond lengths. Distances between the nearest neighbors in a perfect crystal are presented for comparison.

Length	Au	Ag	Pt	Ir
a_{exp}, Å	3.5–4.0 [4] 2.5–4.0 [31] 2.8–3.5 [69] 2.5 [50]	3.3–3.6 [37]	2.8 [21] 2.3 [71]	2.2 [50] 2.2 [71]
a_{calc}, Å	3.1 [72] 2.5–2.9 [68] 2.9–3.1 [70]	3.1 [73] 3.2 [51]	2.8 [74]	2.3 [63]
b_{bulk}, Å	2.9	2.9	2.8	2.7

3.2 Mechanical stresses in atomic contacts

Another important aspect of nanocontact research includes investigation of mechanical properties, such as strain and strength. The surface layers of a crystal may lower the system's energy due to relaxation of atomic layers in the direction normal to the surface or a change in the crystal lattice structure. In the former case, only the interplane distance is altered, while in the latter case periodicity of the crystal structure is disturbed. The surface of any crystal has surface tension. Mechanical stress on the surface is different from zero but vanishes in the bulk. Surface tension is sometimes so high that it may be energetically advantageous to decrease it by rearranging the surface structure or creating surface defects.

Thus, the distribution of strains and stresses is one of the main factors influencing the formation of surface nanostructures. The application of the notions 'strain tensor' and 'stress tensor' in relation to surface nanostructures has some peculiarities. In calculations, the specific stress tensor per atom or hydrostatic stress p_σ is used; the latter parameter is given by the formula [75]

$$p_\sigma = \mathrm{tr}\left\{ -\frac{1}{\Omega_0}\left[\frac{(\mathbf{p}_k)_i(\mathbf{p}_k)_j}{m_k} + \frac{1}{4}\sum_{\substack{l=0\\ l\neq k}}^{N-1}\left((\mathbf{f}_{kl})_i(\mathbf{r}_{kl})_j + (\mathbf{f}_{kl})_j(\mathbf{r}_{kl})_i\right)\right]\right\}, \quad (1)$$

where $\mathbf{f}_{kl}$ is the force acting from atom l on atom k, r_{kl} is the distance between atoms k and l, N is the number of atoms in the system, Ω_0 is the specific volume per atom, and m_k and $\mathbf{p}_k$ are the mass and momentum of atom k, respectively.

Figure 7 exemplifies the dependence of mean hydrostatic stress on the distance between electrodes in a copper 5-atom contact. At the spacing between electrodes equal to 1.1 nm (point A in Fig. 7), the contact is contracted, which accounts for negative mean hydrostatic stress. Contact stretching causes a linear growth of the stress and changes its sign, while the distance between the electrodes increases (point B in Fig. 7). As a result, the nanocontact passes from the contracted state to the stretched one. The stress drops sharply at a certain interelectrode distance (point C in Fig. 7), and the contact breaks down. For a nanocontact with the distance between electrodes at which mean hydro-

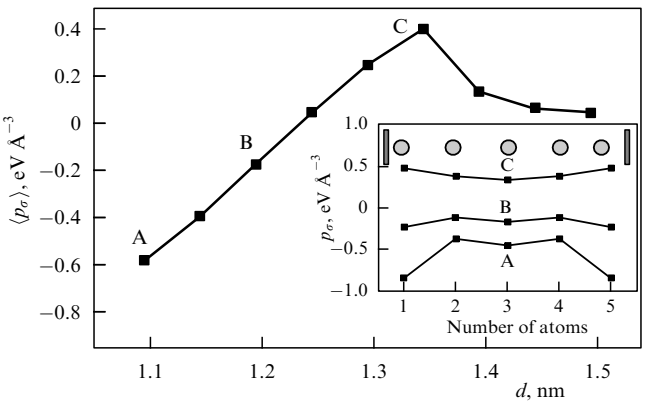

Figure 7. Mean hydrostatic stress $\langle p_\sigma \rangle$ in a coper contact. The inset shows hydrostatic stress on individual atoms of the contact at points A, B, and C [76].

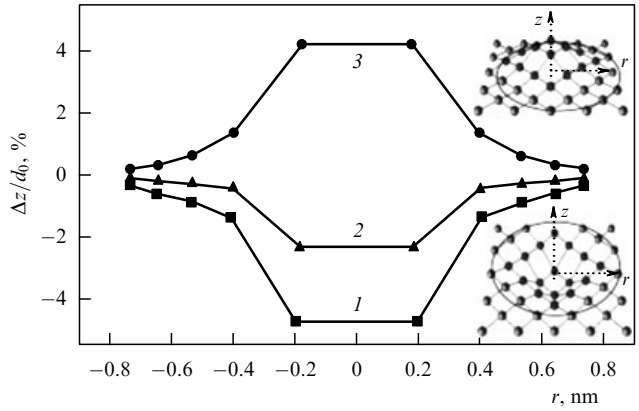

Figure 8. Displacement of copper atoms in electrodes upon contact stretching. Curves *1*, *2*, and *3* correspond to the interelectrode distances 1.1, 1.2, and 1.35 nm, respectively, and $d_0 = 1.8075$ Å. Lower and upper insets depict the electrode surface for curves *1* and *3*, respectively [76].

static stress vanishes, the forces acting on the chain atoms are very small, and the system is energetically more stable than any other one.

Notice the slight inhomogeneity of the local mechanical stress on the atoms of the chain (see the inset to Fig. 7) that is due to the nonuniform distribution of interatomic distances. The bond length, and therefore the stress in the chain, become uniform immediately before the break.

Stretching of a nanocontact is accompanied by deformation of the electrode surface [76]. Figure 8 depicts the displacement of copper atoms in electrodes spaced apart by different distances upon contact stretching. The surface beneath the contact is uneven. When the interelectrode distance equals 1.1 nm, the contact is contracted and its surface becomes concave (curve *1* in Fig. 8). Stretching alters the structure of both the contact and the electrodes. The electrode surface becomes more even when the interelectrode distance is 1.2 nm (curve *2* in Fig. 8). It becomes convex immediately before the break (curve *3* in Fig. 8).

3.3 Young's modulus of nanocontacts and atomic contact breaking force

Evidently, information about elastic characteristics, such as Young's modulus of nanocontacts and atomic contact breaking force, is needed for the practical application of nanocontacts in electronic components. Both quantities strongly depend on geometric dimensions of nanocontacts and temperature [21, 28, 31, 77, 78]. For example, Young's modulus for a gold nanocontact is unrelated to its cross section diameter larger than 30 nm [78] but increases if the diameter decreases from 30 to 1 nm. This change is due to the higher ratio of the number of surface atoms in nanocontacts to the number of bulk atoms at which the surface properties predominate in such systems.

It was found in experiment that Young's modulus for gold nanocontacts varies in the range from 47 to 116 GPa [31]. This means that the maximum value of Young's modulus for a gold nanocontact is 1.5 times that for macroscopic bodies (78 GPa), whereas the inverse is true for Pt [21] and Ag [77].

A wide scatter of Young's modulus values is attributable to the formation of nanocontacts with different structures and crystallographic orientations. Calculations confirm the dependence of Young's modulus on the crystallographic direction along which the nanocontact is stretched out [28]. Young's modulus was shown to decrease with temperature, meaning that nanocontacts tend to undergo plastic strain with rising temperature.

The breaking force of an atomic contact depends on surface orientation and is significantly different from that of a perfect crystal (see Table 1) [45, 47, 51], because the coordination number of the terminal atom depends on the electrode surfaces between which the atomic contact is situated. A change in the coordination number results in an alteration of electronic structure of the atomic contact and, as a consequence, of its interaction with the surface. Therefore, the distance between the terminal atom and the surface, as well as the contact breaking force, may differ for different surfaces [47]. For example, the breaking force for an atomic contact between Au (110) surfaces is 2.2 nN or 3 times that for a crystal (0.7 nN, Table 1). This suggests that the bond strength in metallic contacts is greater than in crystals.

4. Quantum effects in one-dimensional nanostructures

4.1 Density of states in a one-dimensional crystal

Let us consider, before discussing the electronic properties of atomic contacts, such an idealized system as a one-dimensional (1D) crystal in which electrons move freely without interacting with the nuclei (free electron gas).

Let electrons move freely only along the x-axis. The electron energy is quantized in the transverse direction (yz-plane) and takes on discrete values $E_{n_y n_z}$ (electron movements are described, as any two-dimensional motion, by two quantum numbers, n_y and n_z). In this case, the total spectrum is discrete continuous, too, but has only one continuous degree of freedom:

$$E = E_{n_y n_z} + \frac{\hbar^2 k_x^2}{2m} . \tag{2}$$

The number of the allowed states on a $2dk$-long segment for one subzone is equal to the number of cells $2\pi/L$ in length, where L is the crystal length. Therefore, the number of allowed states is defined as

$$\mathrm{d}N = 2\,\frac{L}{\pi}\,\mathrm{d}k\,, \tag{3}$$

where the factor 2 takes account of two admissible values of the spin quantum number for each allowed **k** value.

Expressing the right-hand side of Eqn (3) through energy yields

$$\mathrm{d}N = \frac{1}{\pi\hbar}\sqrt{\frac{2m}{E}}\,\mathrm{d}E\,. \tag{4}$$

The density of states per unit volume for one subzone can be written out using Eqn (4) as

$$\rho^{\,1\mathrm{D}}(E) = \frac{1}{\pi\hbar}\sqrt{\frac{2m}{E}}\,. \tag{5}$$

As mentioned above, there are two limiting directions, y and z, for a one-dimensional system. Therefore, expression (5) needs to be summed over all quantum numbers, n_y, n_z;

hence, one has

$$\rho^{1D}(E) = \frac{\sqrt{2m}}{\pi\hbar} \sum_{n_y, n_z} \frac{\Theta(E - E_{n_y, n_z})}{\sqrt{E - E_{n_y, n_z}}}, \quad (6)$$

where $\Theta(E - E_{n_z})$ is the Heaviside function.

The density of states in the one-dimensional case grows discretely and thereafter falls to the next energy level as $E^{-1/2}$. Such an abrupt increase in density of states and its subsequent decrease occur at each level.

4.2 Density of states in atomic contacts

Let us consider the density of states in atomic contacts. Variations of the structure and size of atomic contacts result in an alteration of their electronic properties. The size of atomic contacts depends on the number of atoms and the interatomic distance. Currently available experimental methods do not permit measuring the density of states in atomic contacts; it has to be found by calculations. Let us consider their results.

To demonstrate the relationship between the contact structure and electronic properties, the authors of Ref. [76] calculated the local density of states in the atoms of a copper contact for its three different states, viz. contracted, stretched, and intermediate. The most pronounced change of the local density of states was observed for s- and d-electrons, whereas that of p-electrons remained virtually unaltered. Therefore, Fig. 9 presents only s- and d-components of the density of states for all atoms of the contact subjected to stretching.

It follows from Fig. 9 that the density of states of atoms in a nanocontact first grows sharply but then gradually decreases. As stressed in Section 4.1, such a behavior of the density of states corresponds to that in an idealized one-dimensional crystal. However, the energy density of atomic states in the nanocontact is more smeared (wider resonance curves) than in the idealized case, since the contact has a finite length and the atoms interact with the electrodes. Figure 9 demonstrates that maxima of the resonance curves are shifted to lower energies. Therefore, nonoccupied electronic states shift to the Fermi level. The shifts are proportional to L^{-2}, where L is the interelectrode distance. This dependence is easy to explain in terms of the particle residing in a quantum box. This model does not exactly describe the particle's behavior in the quantum box, but it explains the shift of the peaks toward low energies with contact elongation.

As pointed out above, density-of-state peaks are shifted toward the Fermi level upon stretching the nanocontact and intersects this level before its break (Fig. 9a). Therefore, the charge density of s-electrons increases, especially in the central atom, which accounts for the enhanced conductance of the nanocontact before its break [79, 80]. States of d-electrons for the atoms of a contracted copper contact are close to the Fermi level and smeared due to strong interatomic interactions (Fig. 9b). Both d- and s-states shift toward lower energies as interelectrode distances increase. The interatomic interaction in a stretched contact is rather weak and the local density of states in terminal atoms is close to that of an atom adsorbed on the surface (adatom) [81].

Thus, d-electrons play the key role in the conductance of contracted copper atomic contacts, whereas s-electrons have a dominant role in the stretched state. In contacts with a small number of atoms, d-states are located closer to the Fermi level than in longer contacts. Moreover, interaction with the surface makes these states smeared in terms of energy. In other words, the number of electrons determining conductance in short contacts is greater than in longer ones, and their conductance is higher. Such a behavior of electronic states is also observed in other atomic contacts possessing a similar electronic configuration, e.g., in gold contacts [80].

Another way to alter the contact length is to vary the number of atoms in it, which changes the density of states in contact atoms. By way of example, Fig. 10a plots the density of states for the central atom of atomic contacts composed of 1–6 copper atoms. It can be seen that the density of states

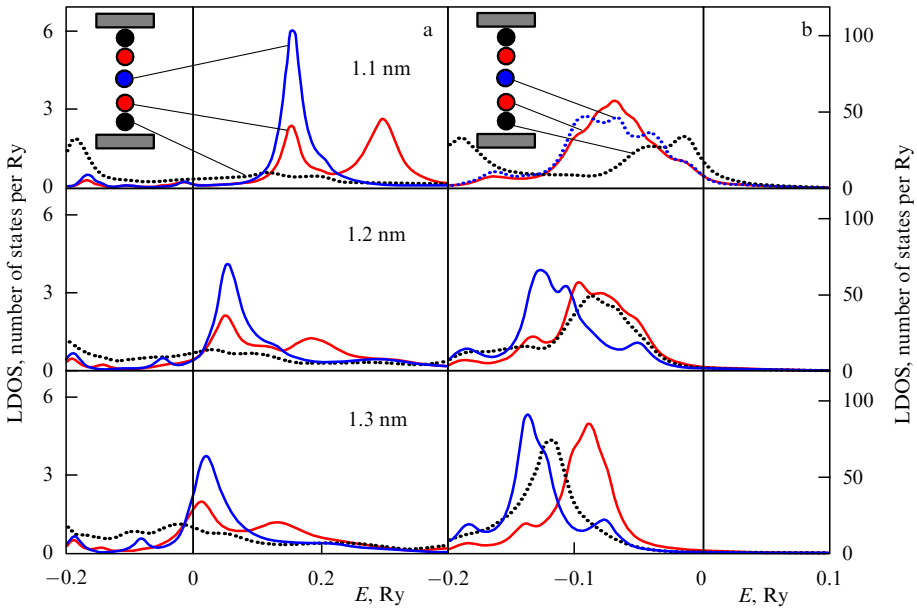

Figure 9. (Color online). Local density of states (LDOS) of s-electrons (a) and d-electrons (b) in copper atoms of a 5-atom contact for interelectrode distances of 1.1 nm, 1.2 nm, and 1.3 nm. Black, blue, and red curves correspond to the local density of states in the terminal atom, central atom, and the atom between the central and terminal ones [76].

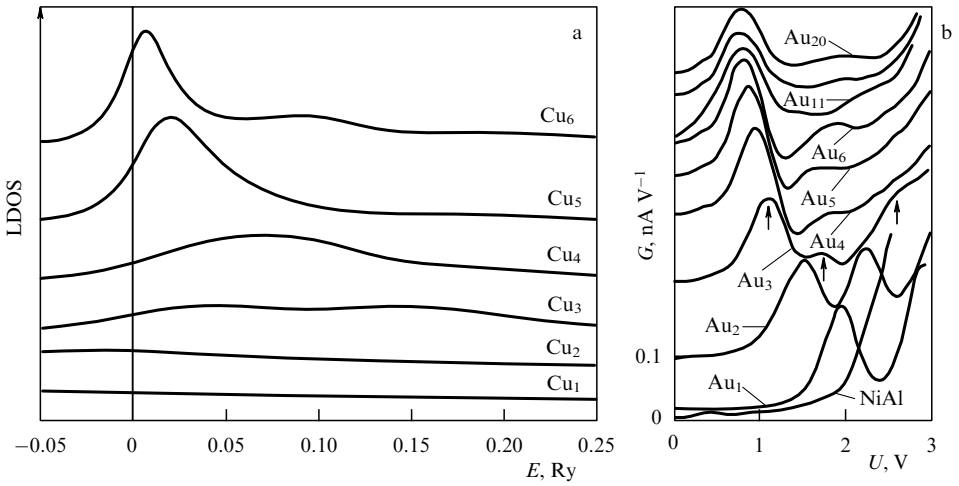

Figure10. (a) Quantum dimensional effect: evolution of the one-dimensional electronic structure in copper contacts; only s-states are presented [76]. (b) Conductance spectra for Au chains of different lengths on the NiAl(110) surface [82].

above the Fermi level increases as the number of atoms in the contact rises. An increase of atoms in the nanocontact gives rise to the number of vacant electronic states and an increased density of states at the Fermi level (Fig. 10a). The observed changes in the density of states suggest the relationship between electronic and mechanical properties of nanocontacts. To recall, similar effects are inherent in other one-dimensional nanostructures, e.g., atomic chains on metallic surfaces [82].

Conductance of Au chains of different lengths on the NiAl(110) surface are shown in Fig. 10b. All the spectra are taken in the center of the chains. The presented experimental and calculated data demonstrate the dependence of electronic properties of the system on its geometry. When comparing these data, the atomic contacts should be considered for equilibrium configurations corresponding to the local minimum of the system's energy rather than prior to break. In so doing, the density of states acquires an oscillating character, as the number of atoms increases in both copper and gold contacts [80, 83].

To sum up, there is correlation between quantum effects and mechanical properties on the atomic scale. Variations of the density of states at the Fermi level related to changes in the contact length strongly affect the conductance of atomic contacts (see Section 5.4 below).

4.3 Spin filter

In recent times, manufacturers of electronic components have undertaken attempts to create devices in which electron spin is utilized as an information carrier. For this purpose, new materials with high spin polarization are needed to function as spin filters that transmit only electrons of a certain spin orientation. The latest publications [84–86] showed that magnetic atomic contacts can be promising materials for spin filters. A quantitative estimation of spin polarization of electron transport through atomic contacts and wires is based on evaluating such characteristics as the degree of spin polarization:

$$P = \frac{T_\uparrow - T_\downarrow}{T_\uparrow + T_\downarrow}\,, \qquad (7)$$

where $T_\uparrow$ and $T_\downarrow$ are the transmission coefficients for spin-up and spin-down electrons, respectively.

It was shown in Ref. [84] that spin-polarized conductance for two-atom Co and Ni contacts is 14 and 45%, respectively, given their ferromagnetic ordering, because in both cases the spin-up electronic states are filled up and their density at the Fermi level is low. At the same time, densities of spin-down electronic states for Co and Ni are at the Fermi level and spin-down electrons make a major contribution to the contact conductance.

Figure 11 exemplifies the density of states in an atomic nickel contact with ferromagnetic and antiferromagnetic ordering of the atoms. Clearly, the density of states at the Fermi level in the latter case markedly increases for spin-up electrons. Moreover, for antiferromagnetic ordering of atoms, the electronic states for a single spin-up atom coincide with those for another, spin-down, atom, which results in the spin polarization vanishing. Such behavior is characteristic of any symmetric system.

The degree of spin polarization of atomic contacts can be enhanced by mixing atoms of 3d- and 5d-metals. For example, Ref. [85] reported that spin polarization of conductance for atomic Pt–Fe wires amounts to 99%. However, it was practically impossible to create nanocontacts with a

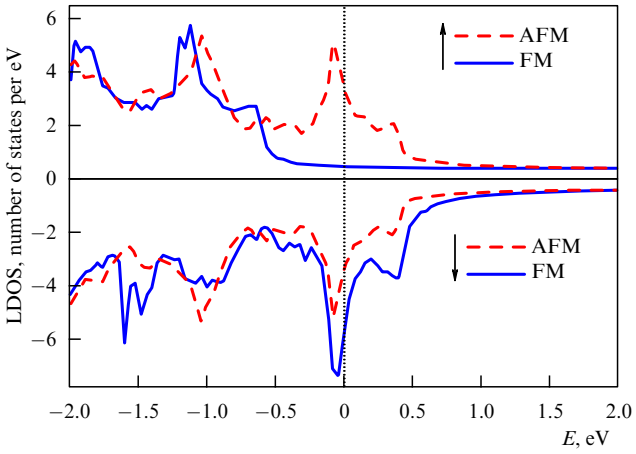

Figure 11. Local density of states in a two-atom Ni contact situated between Ni(001) electrodes for ferromagnetic (FM) and antiferromagnetic (AFM) ordering of atoms in the contact [84].

sequence of Pt–Fe–Pt–Fe atoms. Therefore, the simplest way to increase spin polarization is to form contacts in a gaseous medium. In this case, atoms of gas molecules are built into the contact at the stage of forming the atomic contact and alter its electronic structure (hence, conductance). Even such nonmagnetic metals as Au and Cu may be suitable to create spin filters when they interact with oxygen. Spin-polarized conductance for atomic Au and Cu wires in the presence of oxygen atoms amounts to 17 and 99%, respectively [86].

5. Quantum transport in nanocontacts

5.1 Relationship between electric conductance and transmission function

The classical theory of conduction is inapplicable to one-dimensional systems since it states that conductance G (the inverse of resistance) of a macroscopic conductor is proportional to its cross section area S and inversely proportional to its length L:

$$G = \frac{\sigma S}{L}\,, \tag{8}$$

where conductivity σ is a characteristic of the conductor material.

If the characteristic size of a system is much greater than the electron mean free path, the diffusive conduction regime is described by Ohm's law (8). However, classical Ohm's law is not fulfilled for mesoscopic systems, where quantum effects predominate as, for example, in nanocontacts with a characteristic size much smaller than the electron mean free path. Conductance of such contacts corresponds to the ballistic regime.

Electrons freely propagate in electrodes and resistance is much different from zero only in contacts. The conductance of such nanocontacts is unrelated to their length and is described by the Landauer formula [87]. In the diffusive conduction regime, the length dependence of resistivity in Ohm's law appears as a result of electron scattering in the conductor.

Let us discuss in more detail the ballistic conduction regime [88]. We will consider a one-dimensional conductor (nanocontact) placed between two massive electrodes, a left ('source') one and a right ('sink') one. Current is generated in such a system (contact) only when both the source and the sink reside in local equilibrium and have different electrochemical potentials μ. In this case, the source and the sink are described by two different Fermi functions

$$f_{1,2}(E) \equiv f_0(E-\mu_{1,2}) = \frac{1}{\exp\left[(E-\mu_{1,2})/k_{\mathrm{B}}T\right]+1}\,, \tag{9}$$

where k_{B} is the Boltzmann constant. The difference between electrochemical potentials is proportional to voltage V: $\mu_2 - \mu_1 = -eV$. Under such conditions, the number of electrons in the source is described by the function $f_1(E)$, and in the sink by the function $f_2(E)$. In the stationary state, the number of electrons in the contact is described by a certain intermediate distribution function. Thus, electrons enter the contact through the source, and leave it through the sink. Each contact seeks to restore local equilibrium. This gives rise to a current flow in the external circuit. For the current carried by electrons in the states with positive group velocity v_k, the following expression can be written, taking account of spin degeneracy:

$$I = \frac{2e}{L}\sum_{k,\sigma} v_k\big(f_1(E_k) - f_2(E_k)\big) = \frac{e}{\pi}\int v_k\big(f_1(E_k) - f_2(E_k)\big)\,\mathrm{d}k\,, \tag{10}$$

where L is the contact length, and σ is the electron spin. For a long conductor, summation in formula (10) can be replaced by integration over k. The group velocity is defined as dispersion relation gradient:

$$\hbar\mathbf{v}(\mathbf{k}) = \nabla_k E(\mathbf{k})\,; \tag{11}$$

therefore, for the one-dimensional systems being considered, one obtains $v(k) = (1/\hbar)\,\partial E(k)/\partial k$ and the current will be given by the expression

$$I = \frac{2e}{h}\int \big(f_1(E) - f_2(E)\big)\,\mathrm{d}E \tag{12}$$

showing that each mode per unit energy in a nanocontact carries over current equal to $2e/h$. The total current is zero in equilibrium, because the states with positive and negative velocities are filled equally. The applied voltage V alters the population of energy levels in the interval $E_{\mathrm{F}} \pm (eV/2)$, which leads to a nonequilibrium situation. Evidently, the total current reaches a maximum when the states with positive group velocity are filled to the level with energy $E_{\mathrm{F}} + (eV/2)$, while the states with negative velocity are filled to the level with energy $E_{\mathrm{F}} - (eV/2)$. Therefore, in the energy range

$$E_{\mathrm{F}} - \frac{eV}{2} < E < E_{\mathrm{F}} + \frac{eV}{2} \tag{13}$$

only states with positive velocity well remain. Expression (12) for a conductor with a single energy level takes the form $I = G_0 V$, where conductance quantum $G_0 = 2e^2/h$ is a fundamental constant equal to $(12.9\ \mathrm{k\Omega})^{-1}$.

In a preceding paragraph, the current in the contact was defined as the difference between input and output currents. However, it is useful to consider this current as the difference between two oppositely directed flows coming from the source and the sink. It will give an expression for the current with the use of the transmission function. This approach, sometimes referred to as the Landauer method [88, 89], reduces expression (12) to the following:

$$I = \frac{2e}{h}\int_{-\infty}^{+\infty} \overline{T}(E)\big(f_1(E) - f_2(E)\big)\,\mathrm{d}E\,, \tag{14}$$

where the quantity

$$\begin{aligned}\overline{T}(E) &\equiv \mathrm{tr}\,[\Gamma_1 A_2] = \mathrm{tr}\,[\Gamma_2 A_1] \\ &= \mathrm{tr}\,[\Gamma_1 G \Gamma_2 G^{+}] = \mathrm{tr}\,[\Gamma_2 G \Gamma_1 G^{+}]\end{aligned} \tag{15}$$

is called the transmission function (or coefficient), Γ, A, G, and G^{+} stand for the broadening matrix, spectral function, and retarded and advanced Green's functions, respectively [88]. In this case, a given structure can be regarded as a semipermeable membrane separating two electrodes, and function $\overline{T}(E)$ as describing the penetrability of this membrane for electrons with energy E.

Suppose that a contact connects two uniform electrodes regarded as quantum wires with a large number of modes or energy subzones with well-defined dispersion dependences.

Such an approach makes it possible to determine the S-matrix of the structure, as is done in microwave waveguide problems, where element t_{nm} of the T-matrix describes the transformation amplitude of the mth mode incident on the first electrode and transmitting through the structure into the nth mode at the second electrode. It can be shown that the current is defined in this case by relation (14), with the transmission function expressed as

$$\overline{T}(E) = \sum_m \sum_n |t_{nm}|^2 = \mathrm{tr}\,[tt^+]\,. \tag{16}$$

This approach allows the transmission function to be calculated by studying electron scattering. R W Landauer was the first to apply the theory of scattering as a fundamental tool for conduction research and to demonstrate the relationship between electric conductance and the transmission function: "Conduction is transmission" [87–89]. In this context, the current in a nanocontact assumes, taking account of formulas (9) and (14), the form

$$I = \frac{2e}{h}\int_{-\infty}^{+\infty} \overline{T}(E)\big(f_0(E-\mu_1) - f_0(E-\mu_2)\big)\,\mathrm{d}E\,. \tag{17}$$

In equilibrium, the current is zero, because $\mu_1 = \mu_2$. Low voltage applied to two electrodes changes each of the $\overline{T}$, μ_1 and μ_2, functions. As a result, in the first approximation one arrives at

$$I \approx \frac{2e}{h}\int_{-\infty}^{+\infty} \delta\overline{T}(E)\big(f_0(E-\mu_1) - f_0(E-\mu_2)\big)\,\mathrm{d}E + \frac{2e}{h}\int_{-\infty}^{+\infty} \overline{T}(E)\,\delta\big(f_0(E-\mu_1) - f_0(E-\mu_2)\big)\,\mathrm{d}E\,. \tag{18}$$

The first integral on the right-hand side of the last formula is zero, while the second one can be presented as

$$I \approx \frac{2e^2V}{h}\int_{-\infty}^{+\infty} \left(-\frac{\partial f_0(E)}{\partial E}\right)_{E=\mu} \mathrm{d}E\,; \tag{19}$$

therefore, conductance is described by the Landauer formula

$$G = \frac{2e^2}{h}\,T_0\,, \quad \text{with} \quad T_0 \equiv \int_{-\infty}^{+\infty} \overline{T}(E)\,F_T(E-\mu)\,\mathrm{d}E\,, \tag{20}$$

where function $F_T(E-\mu)$ defines thermal broadening. Function F_T has a sharp peak of width $k_\mathrm{B}T$ near $E = \mu$, meaning that conductance is proportional to the transmission function averaged over the energy interval equal to a few $k_\mathrm{B}T$ near the equilibrium chemical potential μ.

The maximum value of the transmission function (therefore, conductance) is reached when each of the M subzones or modes of one electrode ideally transfers charges into the other electrode. In this case, matrix $[tt^+]$ is a diagonal matrix $M \times M$ in size with unities on the main diagonal, and the transmission coefficient is M. In other words, the maximum transmission coefficient is equal to the number of modes inherent in the electrode.

5.2 Changes in nanocontact conductance upon stretching

An increase in the interelectrode distance up to the value at which nanocontacts break down results in a change to both their structure and conductance. Alteration of conductance and elastic forces in gold nanocontacts upon their stretching at 4.2 K is demonstrated in Fig. 12a showing a discrete variation of conductance, with each of its values (plateaus) being a multiple of conductance quantum $G_0 = 2e^2/h$. Each such transition is accompanied by a jump of the nanocontact elastic force. The last plateau is equal to G_0 and corresponds to a linear atomic contact. Such conductance behavior of the nanocontact is characteristic of all metallic nanocontacts [4, 15, 21, 33, 34, 36, 71].The jump-like behavior of nanocontact conductance is largely due to the rearrangement of the atomic structure. Results of calculations of nanocontact conductance using the MD method to determine the contact structure reveal a correlation between elastic force oscillations and changes in conductance upon stretching [26, 38, 90–92]. Further experimental observations have every time given a different length of the conductance plateau, since it has proven impossible to control an atomic configuration in the contact.

The transition from one conductance plateau to another at a low temperature depends on the direction in which the distance between electrodes changes and has the form of a hysteresis loop (Fig. 1b). Conductance hysteresis is observed within a narrow range of interelectrode distance variations (on the order of tenths of an angström) and vanishes as the temperature rises [12, 15], since each conductance plateau

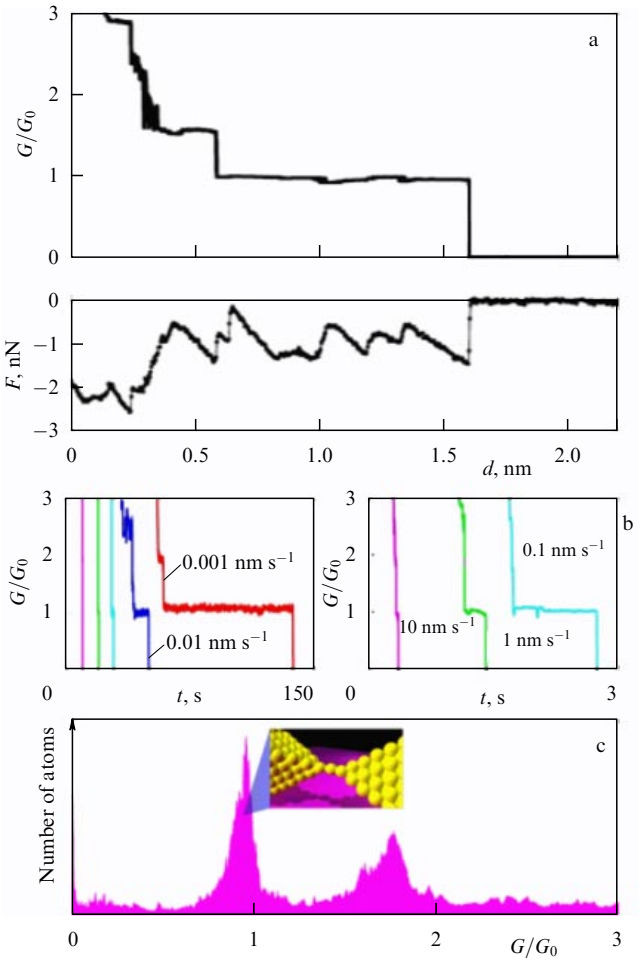

Figure 12. (a) Conductance and elastic force measured while stretching a gold nanocontact at 4.2 K [25]. (b) Typical conductance curves obtained upon stretching nanocontacts with different rates. (c) Conductance histogram of gold nanocontacts obtained for the break of 1000 nanocontacts at a rate of 10 nm s^{-1} [93].

corresponds to a specific local minimum. The higher the energy barrier between two atomic configurations, the higher the temperature at which conductance hysteresis disappears. Hysteresis is absent in constant conductance regions, when the nanocontact is in the elastic phase and can return to the original configuration along the same path. Moreover, hysteresis is not observed at room temperature.

It is difficult to prepare nanocontacts with equal interatomic distances under experimental conditions. Therefore, experimentally obtained contacts have different atomic configurations, which makes it impossible to study the dependence of their conductance on the interatomic distance. For this reason, a statistical approach to constructing conductance histograms is usually employed for more objective analysis of the available data. To this end, a large number of conductance measurements have been made upon contact stretching [37]. Since the sample size is large, all atomic configurations or effective dimensions of nanocontacts are equally probable. Therefore, conductance peaks can be expected to occur for those configurations that form more frequently than others.

The interatomic distance dependence of conductance illustrated by Fig. 12 [25, 93] suggests that peaks in the conductance histogram (Fig. 12c) correspond to the distances at which the conductance plateau is observed. Although this approach fails to completely characterize the nanocontact, it makes possible investigation of quantum effects of conductance at both low and room temperatures. Usually, thousands of conductance curves like those presented in Figs 12a, b are measured for certainty. The figure shows that the time of existence of an atomic contact strongly depends on its stretching rate.

To recall, statistical analysis of results with the aid of conductance histograms was first applied by Russian researchers [94], although a later publication by Olesen et al. [95] is usually cited.

5.3 Characteristic time dependences of metallic atomic contact conductance

Transition from one conductance plateau to another is possible by jump-like variation of conductance, as shown in Fig. 13a. Such variation occurs at both low [96] and room [91, 97] temperatures. In certain cases (Fig. 13b), a more gradual transition from one conductance plateau to another is observed [98–100]. Sometimes, the time dependence of nanocontact conductance is accompanied by shot noise (Fig. 13c) [98, 101, 102]. Shot noise with a high amplitude close to G_0 for a superconducting Nb nanocontact was shown in Ref. [102] to be related to the reversible opening of the conduction channel, which is, in turn, associated with a change in the density of states during dimerization of nanocontact atoms. Such conductance behavior in gold atomic contacts is due to fluctuations of the system between its metastable states having different conductance [101].

Results of computer simulation indicated that stretching a nanocontact [98] or the formation of atomic contacts in the course of self-organization [29, 30] may give rise to two system's states with similar energy and different conductances. This, however, is not always possible to observe in experiment, first of all due to timing constraints on conductance measurements. Such phenomena can be explained in terms of three important temporal characteristics.

The first such characteristic, the time of transition t_{sw} between two metastable atomic configurations of the nanocontact, is described by the expression

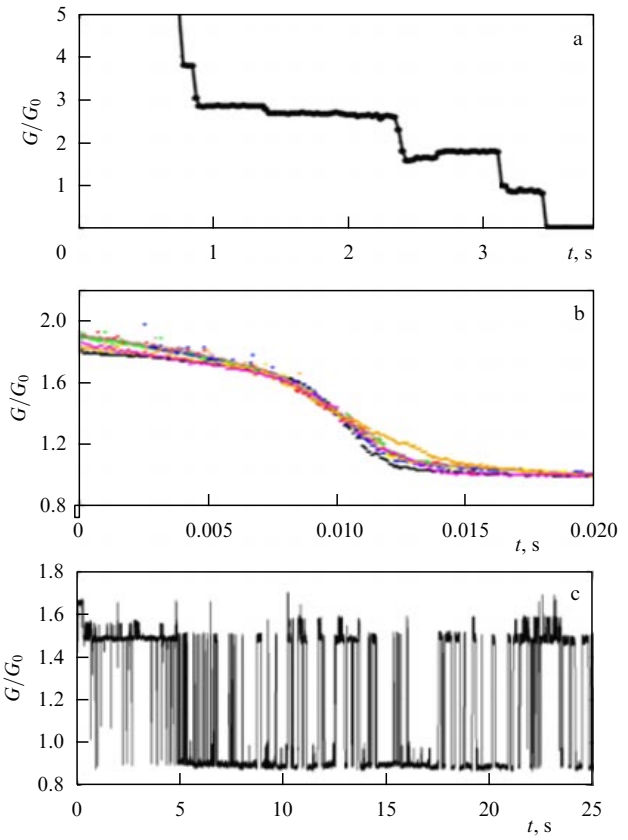

Figure 13. Characteristic time dependences of conductance of gold atomic contacts: (a) a jump in conductance upon transition from one plateau to another [91]; (b) gradual transition from one plateau to another upon stretching at a rate of 100 nm s^{-1}, and (c) shot noise in the time dependence of conductance.

$$t_{sw} = \frac{1}{v_0} \exp\left(-\frac{E_b}{k_B T}\right), \tag{21}$$

where E_b is the energy barrier between metastable atomic configurations, v_0 is the frequency pre-factor, and T is temperature.

The second temporal characteristic is the measuring time t_{sa}. The third one is time t_c during which metastable atomic structures exist, given by the ratio of the change in the nanocontact length to the stretching rate.

The relationship among these three variables determines the character of the measured conductance. The timing diagram in Fig. 14 illustrates three characteristic shapes of time dependence of conductance for gold nanocontacts undergoing stretching. The first region is the largest one, and the time of existence of metastable atomic configurations in it, t_c, is shorter than the time of transition between them, t_{sw}, or shorter than conductance measurement time, t_{sa}. Such a relationship between characteristic times obeying inequalities

$$\begin{aligned} &t_{sa} > t_c > t_{sw}\,, \\ &t_{sw} > t_c > t_{sa}\,, \\ &t_{sa} > t_{sw} > t_c\,, \\ &t_{sw} > t_{sa} > t_c \end{aligned} \tag{22}$$

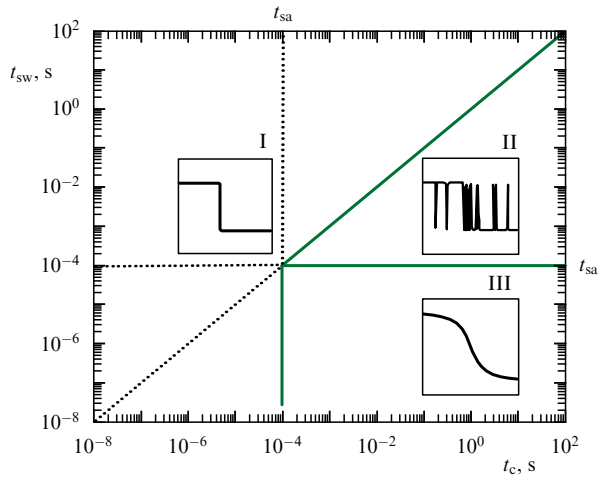

Figure 14. Timing diagram (t_{sw}, t_{sa}, and t_c) illustrating three characteristic conductance regions. Diagonal line $t_{sw} = t_c$, vertical line $t_{sa} = t_c$, and horizontal line $t_{sw} = t_{sa}$ are plotted. The insets show schematically the time dependences of conductance for gold atomic contacts in a given region [98].

is associated with sharp variations of conductance. In the second and third regions, the time of existence of metastable atomic configurations, t_c, is longer than the time of transition between them, t_{sw}, and longer than conductance measurement time, t_{sa}. Moreover, conductance measurement time t_{sa} in the second region is shorter than time t_{sw} of transition between atomic metastable configurations, namely

$$t_c > t_{sw} > t_{sa} . \tag{23}$$

In this case, shot noise appears in the time dependence of conductance. The third region is given by the inequality

$$t_c > t_{sa} > t_{sw} , \tag{24}$$

and a gradual transition from one conductance plateau to another is observed in it, because mean conductance is recorded in experiment.

5.4 Atomic contact conductance

Now, let us consider at greater length the characteristic features of atomic contacts. Figure 15 presents a histogram of platinum atomic contact lengths, where the solid curve traces an approximation of experimental data by the Gaussian function. The lower part of the figure illustrates the dependence of conductance on the length of atomic contacts composed of 3 to 6 atoms. Obviously, the conductance of metallic atomic contacts decreases with an increase in the number of atoms, as was reported for the first time in experimental papers [21, 71] and explained theoretically in Refs [83, 103]. Such a conductance behavior is related to the overlapping of electron shells in contact atoms (the smaller the number of atoms, the greater the electron shell overlap in both contact and electrode atoms). When the number of atoms in the contact increases, their interaction with electrode atoms diminishes, which leads to a decrease in the number of conduction channels and, therefore, of conductance itself. After a further increase in the number of atoms, only one or two conduction channels remain, and the conductance no longer varies. Notice that conductances calculated for nanocontacts with flat electrodes [104] are significantly different from those for contacts with pyramidal-shaped electrodes [103].

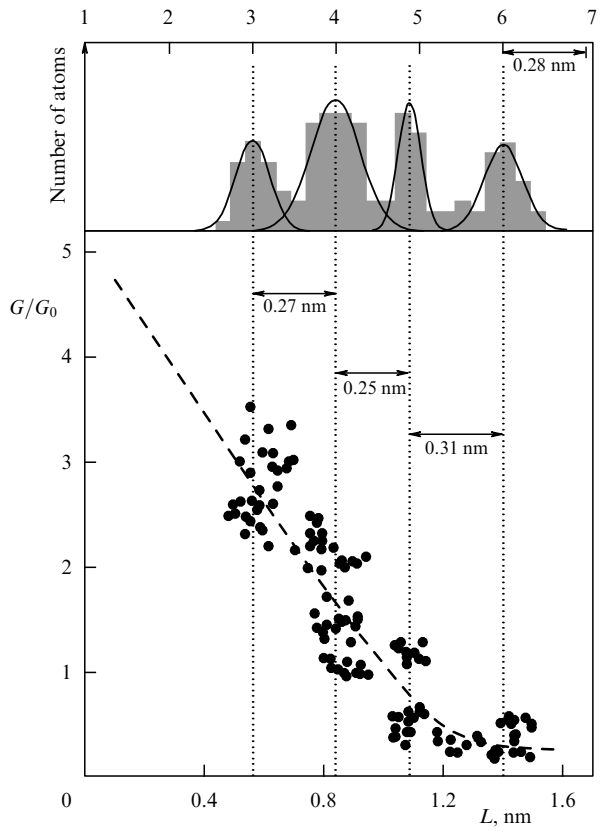

Figure 15. Histogram of the number of atoms in an atomic contact (top) and the dependence of conductance of a Pt atomic contact on its length L (bottom) [21].

Calculations in the framework of the density functional theory and the one-dimensional model of free electrons have revealed fluctuations of conductance with an amplitude of 3% depending on the number of atoms [71, 80, 83]. For example, the slightest change in the structure of atomic contacts composed of univalent atoms (Na, Cu, Ag, Au, etc.) alters the density of states at the Fermi level. It was shown in Ref. [83] for a copper atomic contact that the maxima in the density of states (therefore, of conductance) at the Fermi level occur in contacts with an odd number of atoms, and minima in contacts with an even number of atoms. The physics of this effect is related to quantum interference of electron waves propagating through the atomic contact and waves reflected from the contact–electrode interface.

In the foregoing, we considered systems with the degenerate energy state of electrons having different spin orientations in atomic contacts, which accounted for equal partial spin-polarized currents and a resultant jump in conductance equaling $2e^2/h$. Spin degeneracy is removed in magnetic atomic contacts and the density of states at the Fermi level differs for electrons with different spin orientations. In this case, the probability of tunneling in an external magnetic field for electrons with different spin orientations is different, too, and the motion of electrons with unidirectional spins to which jump e^2/h corresponds predominates.

Unexpectedly, the conductance of 3d-, 4d-, and 5d-electron metallic atomic contacts was found to equal e^2/h in the absence of a magnetic field at room temperature, which suggests the flow of spin-polarized current through these structures [21, 33, 105]. Even more surprising is the fact that

nonmagnetic Au, Pd, and Pt form atomic contacts with conductance e^2/h, which gives indirect evidence that they become magnetic. Low-temperature experiments carried out in the absence of an external magnetic field have failed to show a conductance peak of e^2/h for nanocontacts composed of Fe, Co, Ni, and Pt atoms [106]. Such conflicting results gave reason to conclude that the atomic contacts under consideration contained not only metal atoms from which they were formed but also impurities [57, 106, 107]. The conductance of metallic nanocontacts containing atomic impurities proved much lower than G_0 [108–112]. It did not decrease at low temperatures if it was possible to store samples free from impurities during a long enough period.

A different explanation of such fractional conductance in nonmagnetic contacts was proposed in theoretical studies [113, 114]. The authors considered a one-dimensional model of quantum ballistic contact represented in the form of a potential barrier with electron–electron interaction localized in it. They showed that strong enough interactions gave rise to a state with spontaneous spin polarization [114]. This state was metastable, which enabled the system to remain in this state only at high temperatures.

Of no small importance is the influence of a magnetic field on the conductance of nanocontacts. The occurrence of ballistic anisotropic magnetoresistance in ferromagnetic contacts was predicted in Ref. [115]. It is due to electron scattering anisotropy as a result of spin–orbit interaction. The ballistic anisotropy of magnetoresistance for Ni nanocontacts is estimated at 17%, which is an order of magnitude higher than for bulk ferromagnets.

The first experimental measurement of ballistic anisotropic magnetoresistance in Co nanocontacts was reported in Ref. [116]. A Co nanocontact was placed here on a silicon substrate (Fig. 16a) and rotated about its axis in a magnetic field. The conductance changed abruptly as the angle between the magnetic field direction and the sample plane varied during the rotation. The changes in conductance equaled e^2/h, $2e^2/h$, and sometimes $4e^2/h$.

The dependence of nanocontact conductance on the angle between the magnetic field direction and the sample plane is illustrated in Fig. 16b. It was shown in the framework of the tight-binding model that the said jumps of conductance result from a change in the number of electron subzones intersecting the Fermi surface and associated with alteration of the band structure in the magnetic field [116]. Such an effect of jump-like variation of conductance upon a slight change in magnetization direction can be used in memory sensors and magnetic memory devices.

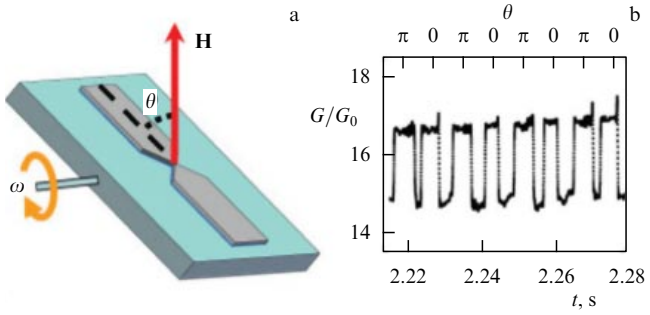

Figure 16. (a) Layout of experiment. (b) Dependence of conductance on time and angle θ measured with respect to the electrode plane. Angle θ changes from 0 to π. Magnetic field induction $B = 1$ T, and the period of rotation of the sample $T = 20$ s [116].

6. Magnetism in one-dimensional nanostructures

According to Lieb and Mattis theorem [117], the ground state of 1D systems is nonmagnetic. However, neither atomic nanowires nor nanocontacts are strictly one-dimensional systems. Therefore, some of them are magnetic. The coordination number and the interatomic distance are two main parameters determining the magnetic moment of a nanosystem. A decrease in coordination number or an increase in interatomic distance are responsible for the enhancement of the magnetic moment of nanocontact atoms. In certain cases, variation of these parameters may be exploited (see below) to convert nonmagnetic metals of a perfect crystal into magnetic ones in atomic contacts.

6.1 Magnetic properties of atomic contacts in 3d-metals

To begin with, let us consider the magnetic properties of infinite nanochains. Calculations in the framework of the density functional theory have shown that the magnetic properties of one-dimensional nanochains are closely dependent on interatomic distances, while their changes depend on the electronic structure [62, 118, 119]. Table 3 presents spin magnetic moments for the atomic chains of 3d-, 4d-, and 5d-metals in which the interatomic distances correspond to the system's energy minimum [55, 62, 63, 74, 118–121]. Of all 3d-metals, only Cr and Mn atoms exhibit antiferromagnetic ordering in wires. All other metals experience ferromagnetic ordering of atoms [62].

The interatomic distance dependence of spin and magnetic moments for the atomic chains of 3d-metals has the following form. A wire with small interatomic distances is

Table 3. Spin magnetic moments (in μ_B units) for infinite atomic chains of 3d-, 4d-, and 5d-metals.

3d			4d			5d		
Ti	0.45	[62]	Zr	0.63	[63]	Hf	2.60	[63]
V	1.00 – 1.57	[62, 118, 120]	Nb	—		Ta	—	
Cr	1.95	[62]	Mo	1.32	[63]	W	1.47	[63]
Mn	4.06 – 4.40	[62, 118, 119]	Tc	1.27	[63]	Re	1.73	[63]
Fe	3.26 – 3.30	[62, 118, 119]	Ru	1.11 – 1.12	[63, 121]	Os	—	
Co	2.18 – 2.26	[62, 118, 119]	Rh	0.30 – 0.33	[63, 121]	Ir	0.66	[63]
Ni	1.14	[62, 118]	Pd	0.68 – 0.70	[55, 63, 121]	Pt	1.10	[74]

paramagnetic due to a strong overlap between 3d-orbitals; in other words, its magnetic moment is zero [119]. A further increase in the interatomic distance turns the nanowire into a ferromagnetic structure and enhances the magnetic moment of atoms. At very large interatomic distances, the atoms become free, and their magnetic moments correspond to the magnetic moments of free atoms. For example, the spin magnetic moment of atoms in a Co atomic wire with interatomic distances smaller than 1.5 Å is zero. It increases to $2.3\,\mu_B$ for the interatomic distance of 2.2 Å, corresponding to the equilibrium configuration of the wire [119], but remains lower than $3\,\mu_B$ in a free Co atom.

Low-dimensional structures are known to have a well apparent direction in which their physical properties are significantly different from those in other directions. For this reason, strong magnetic anisotropy is most likely to exist in such structures, an example being linear atomic wires with two characteristic directions: one along the wire axis, the other across it. In this connection, let us consider the anisotropy of magnetic properties of atomic wires.

The anisotropy of the spin magnetic moment for the 3d-wire atoms is negligibly small, and the difference between spin moment projections onto the axis of light and heavy magnetization directions is $0.001\,\mu_B$ [122]. The absence of spin magnetic moment anisotropy is also characteristic of the atoms of small surface clusters [123]. Unlike spin magnetic moment anisotropy, the anisotropy of the orbital magnetic moment of the atoms in wires fabricated from 3d-metals is rather high [122] due to its, as a rule, maximum projection onto the light magnetization axis in transition metals with a more than half-filled d-subshell. For example, projections of the orbital moment onto the direction parallel to the axis of Fe and Ni wires are $0.42\,\mu_B$ and $0.45\,\mu_B$, respectively, or several times those onto the direction perpendicular to the axis ($0.15\ \mu_B$ and $0.12\ \mu_B$). For all 3d-metals, except Ti, Mn, and Co, the light magnetization axis coincides with the wire axis. The magnetic anisotropy energy of 2.65 and 5.19 meV per atom for Co and Fe atomic wires, respectively [122] is several-fold higher than that for Co and Fe monolayers on the surface of the metals (1.86 and 0.20 meV per atom) [124]. Ni atomic wires have the highest magnetic anisotropy energy of 11.44 meV per atom [122]. It has recently been shown that the magnetic anisotropy energy for Co atomic wires can be increased from 2.65 to 140 meV per atom by mixing Co and Au atoms [125]. Therefore, atomic Ni wires and mixed CoAu wires are the most promising materials for producing magnetic memory devices with a high recording density.

However, an atomic wire represents too idealized one-dimensional system, because the real surface influences the properties of atomic structures. The magnetic properties of an atomic contact composed of Co atoms residing between copper electrodes are described in Ref. [126]. A change in the interelectrode spacing alters interatomic distances in the contact differently in the center and between the terminal atom and an electrode. Lengthening of the contact is largely due to the growing distance between the terminal atom and an electrode, whereas the interatomic distance in the center of the contact increases insignificantly.

The results of calculations in the framework of the density functional theory, obtained in Ref. [126], indicate that atoms in the vicinity of electrodes have smaller spin magnetic moments than central atoms by virtue of their higher coordination numbers. Interaction between the d-states of a cobalt atom and the sp-states of the nearest copper atoms of an electrode lowers the spin magnetic moment. Due to enhanced hybridization with electrode atoms, the Co atoms are more sensitive to variations of the interelectrode distance. In an atomic contact being stretched, the increase in the spin magnetic moment of an atom close to the electrode is more pronounced than in the central atom. Such changes of bond lengths and spin magnetic moments are also inhered in longer contacts. The length of interatomic bonds in the center is 2.3–2.4 Å, the distance between an electrode and the terminal atom varies from 1.8 to 2.1 Å, and spin magnetic moments are 2.2 and $1.8-2.0\,\mu_B$, respectively. For comparison, the spin magnetic moment of an adatom and atoms in small Co clusters on the Cu(100) surface equals $1.8\,\mu_B$. This means that spin magnetic moments of atoms in the contact are higher than on the surface but lower than those of free atoms.

A detailed analysis of the density of states revealed marked changes in the electronic states of magnetic atomic contacts as the number of their atoms increased [126]. A comparison of d-states for a monatomic Co contact and the central Co atom in a three-atom contact showed that the d-states for spin-up electrons are filled in both cases, and the densities of these states are virtually identical. At the same time, the density of spin-down states for cobalt is at the Fermi level; it accounts for a marked change in the density of these states. Decreased interaction of the central atom with the neighboring atoms and electrode atoms results in a split of the density of spin-down states at the Fermi level for the central atom of a three-atom contact. Therefore, the slightest change in the structure or the interatomic distance may significantly alter the density of spin-down states.

The variation in the density of spin-down and spin-up electrons at the Fermi level is depicted in Fig. 17a. It can be seen that changes in the density of spin-down electrons are especially well apparent and occur periodically. The density of states for contacts with an odd number of atoms has a minimum and that for contacts with an even number of atoms exhibits a maximum due to the formation of dimers in the contacts. In the case of an odd number of atoms, the central position is occupied by an atom, and in contacts with an even number of atoms by a dimer. The formation of dimers changes the position of the density of states for spin-down electrons and increases the density of states at the Fermi level. Oscillations of the density of states lead not only to oscillations of conductance in atomic contacts but also to the alteration of spin magnetic moments of the central atom in the range of $(1.9-2.2)\,\mu_B$ (Fig. 17b).

6.2 Magnetic properties of atomic contacts in 4d- and 5d-metals

Because both theoretical and experimental research have shown that nonmagnetic 4d- and 5d-metals become magnetic as free clusters and small clusters on the surface of noble metals [127, 128], it is of interest to study the magnetic properties of one-dimensional systems based on 4d- and 5d-metals.

Magnetism in 4d and 5d systems strongly depends on such characteristics as symmetry, coordination number, and interatomic distance. An example is provided by magnetism in Pd atomic contacts. A palladium cluster on a copper surface is a nonmagnetic entity, just likes nanocontacts, but their stretching gives rise to an atomic contact whose atoms acquire a magnetic moment [55, 126, 129]. Notice also that the

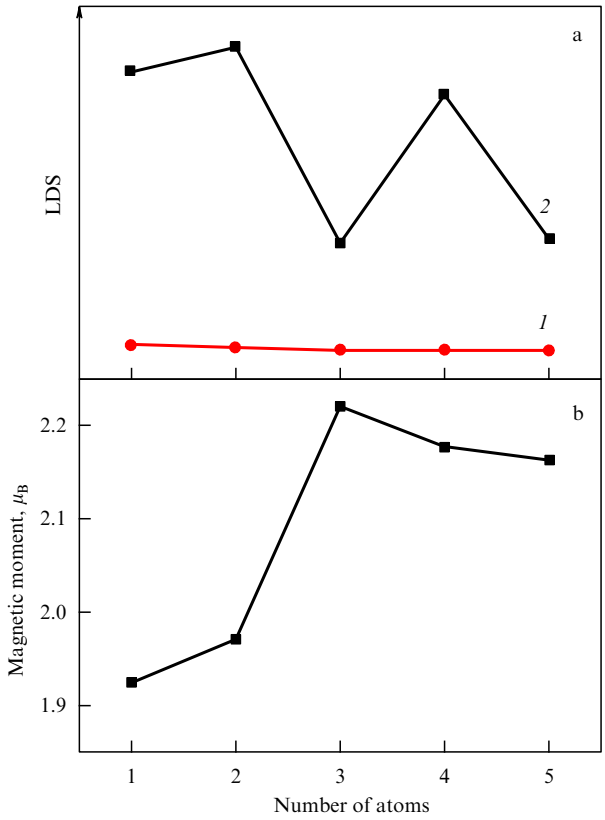

Figure 17. (a) Local density of states for spin-down electrons (curve *1*) and spin-up electrons (curve *2*) at the Fermi level of the central atom in a contact composed of 1–5 Co atoms. (b) Magnetic moment of the central atom in a contact composed of 1–5 Co atoms [126].

influence of atomic relaxations on 4d-system magnetism is much stronger than in 3d systems due to the greater extent of 4d-wave functions.

Let us begin with considering an infinite chain of Pd atoms. The authors of Ref. [129] were the first to show theoretically in the framework of the generalized gradient approximation that the spin magnetic moment of atoms spaced 2.3–3.4 Å apart in an atomic wire can be as high as $0.7\,\mu_B$, and the energy of the ferromagnetic state (12 meV per atom) is lower than the energy of the paramagnetic state [129]. The values of spin magnetic moments in wires of other 4d- and 5d-metals are listed in Table 3.

However, later authors questioned the existence of magnetism in an infinite chain of Pd atoms on the grounds that the paramagnetic state is energetically more advantageous in terms of the local density approximation [130]. Such a discrepancy in the magnetic properties of atomic palladium wires arises from the fact that interatomic distances corresponding to the equilibrium configuration of a system differ in the framework of different approximations. For example, it was shown in Refs [53, 55] that the equilibrium interatomic distance in the wire equals 2.34 Å in the framework of the local density approximation, but 2.44 Å in the framework of the generalized gradient approximation. In other words, the difference between interatomic distances explains why a wire is magnetic in one approximation, and nonmagnetic in another [55].

Spin magnetic moment anisotropy for 4d- and 5d-metallic atomic wires has acquired significance, unlike that for 3d ones, with the difference between the spin magnetic moments amounting to $0.2\,\mu_B$ [63]. The projection of the atom's orbital momentum in the wire onto the light magnetization axis is several times that onto the heavy magnetization axis, as in 3d-metals. Simultaneously, the energy of magnetic anisotropy in atomic wires of 4d- and 5d-metals is an order of magnitude higher than in 3d-metals. For example, the energies of magnetic anisotropy for Ru and Rh are 12 and 7 meV per atom, compared with 60 and 11 meV per atom for Re and Ir, respectively [63].

To continue discussing the magnetic properties of palladium atomic contacts, we refer to Refs [55, 126], where their magnetic properties were considered for the first time taking account of atomic relaxation. The spin magnetic moment of the central atom in the three-atom contact is $0.3\,\mu_B$, while the distance between the central and terminal atoms is 2.5 Å. The spin magnetic moment of surface atoms ($0.1\,\mu_B$) is one third that of the central atom. The diminishing of the magnetic moments of the terminal atoms is due to interaction with electrodes.

Analyses of charge distribution in atomic contacts show that the existence of magnetic moments is caused by sd-hybridization which abruptly diminishes the number of d-electrons around a palladium atom. Similar property is characteristic of free palladium clusters as well [127]. Calculations of the total energy of three-atom palladium contacts demonstrate that the difference between energies of ferromagnetic and paramagnetic states is only +6 meV per atom, when the contact is located between copper electrodes [126], and −3 meV per atom when the contact resides between palladium electrodes [55]. Nanocontacts being metastable systems, even slight structural changes, a rise in temperature, or other factors may cause a transition of the palladium contact from the nonmagnetic to the magnetic state and vice versa. It is possible to increase the difference between the energies of ferromagnetic and paramagnetic states, and thereby to enhance the stability of the magnetic contact, by introducing impurities [64].

As far as other metals are concerned, the energy of a rhodium ferromagnetic contact is by 67 meV per atom lower than that of a paramagnetic contact [126]; in other words, the difference is much greater than for palladium. The magnetic moment for the central atom of a rhodium atomic contact is $1.47\,\mu_B$. For comparison, the atoms of an atomic wire in the absence of electrodes have a spin magnetic moment of $0.30\,\mu_B$ (see Table 3). The magnetic moment of atoms close to the electrodes drops to $0.38\,\mu_B$, i.e., becomes one quarter of the central atom.

To recall, atomic relaxations and interactions with electrodes result in the nonuniform distribution of magnetic moments inside a contact; moreover, the magnetic properties of the contacts in a relaxed geometry [55, 126] are substantially different from those of idealized contacts [129].

7. Conclusion

The analysis of numerous experimental data presented in this review showed that TEM constitutes the simplest method for the formation and visualization of atomic contacts, whereas the mechanically controllable break junction technique is most suitable for electric conduction research. However, the latter method does not guarantee the formation of good atomic contacts for all metals. Therefore, TEM is thus far the sole available method for creating atomic contacts for technical applications.

The molecular dynamics method is the main tool for simulating atomic contact formation allowing calculations for cells with tens of thousands of atoms to be made. An important disadvantage of this method is that it cannot be used to simulate the evolution of nanocontacts less than 10 fs in duration. Although the kinetic Monte Carlo method is extensively used to simulate self-organization of nanostructures on metallic surfaces, it has only recently found wide application in research concerning the formation of atomic contacts, in the first place because strain in nanocontacts is much more pronounced than in nanostructures on the metal surface. Combining these two methods made it possible to obtain new data; specifically, it revealed different mechanisms underlying the formation of atomic contacts upon stretching a nanocontact and the evolution of a narrow passage between two holes.

Both experimental and theoretical studies of the mechanical properties of nanocontacts have shown that stretching a contact triggers a sequential formation of elastic and inelastic phases. In this case, interatomic distances in metallic atomic contacts can be much greater than in crystals, and the breaking force for an atomic contact can be several times that for a crystal.

The analysis of atomic contacts demonstrated a correlation between quantum effects and mechanical properties. For example, the jump-like conductance in nanocontacts is due to rearrangement of the atomic structure in which the character of transition depends on the relationship among atomic configuration lifetime, transition time between atomic configurations, and conductance measurement time. The accompanying oscillations of conductance are related to an increase in the number of atoms in the contact, and to oscillations of the density of states at the Fermi level. It is possible to control conductance in magnetic nanocontacts not only by varying their length but also by applying an external magnetic field.

The energy of magnetic anisotropy in atomic contacts is several-fold higher than in monolayers and small clusters at the surface. The conductance of magnetic atomic contacts is spin-polarized, with the degree of spin polarization being 45%. It is possible to increase the magnetic anisotropy energy of an atomic contact by an order of magnitude and the degree of spin polarization up to 99% by introducing impurities in the form of atoms of other metals or light gases.

Further progress in atomic contact research requires substantial improvement of both experimental techniques and computation methods. Advances in nanocontact technology imply the development of contacts with fully predictable chemical compositions. The mainstream development path for computer-assisted investigations into the properties of atomic contacts is associated with the exploitation of supercomputers.

The unique properties of atomic contacts make them a promising material for technological applications. Specifically, the large magnetic anisotropy of atomic contacts opens up prospects for their use in magnetic memory devices with high recording density. Atomic contacts with a high degree of spin polarization may find application for the creation of spin filters, while the anisotropic magnetoresistance effect can be employed for the development of sensors. However, practical applications of atomic contacts are hampered by their poor stability. Therefore, prolonging the lifetime of nanocontacts is a priority task facing researchers in this field.

Acknowledgments

The authors are grateful to all their colleagues affiliated with Lomonosov Moscow State University. Special thanks are due to S V Kolesnikov, K M Tsysar, and E M Smelova. The work was partially supported by the Russian Foundation for Basic Research (grant No. 15-32-20560).

References

1. Ignatov A N *Nanoelektronika. Sostoyanie i Perspektivy Razvitiya* (Nanoelectronics. State-of-the-Art and Prospects for Further Development) (Moscow: Flinta, 2012)
2. Chaplygin Yu A (Ed.) *Nanotekhnologii v Elektronike* (Nanotechnologies in Electronics) (M.: Tekhnosfera, 2013)
3. Paul W, Oliver D, Grütter P *Phys. Chem. Chem. Phys.* **16** 8201 (2014)
4. Ohnishi H, Kondo Y, Takayanagi K *Nature* **395** 780 (1998)
5. Agraït N, Rodrigo J G, Vieira S *Phys. Rev. B* **47** 12345(R) (1993)
6. Costa-Krämer J L et al. *Phys. Rev. B* **55** 5416 (1997)
7. Olesen L et al. *Phys. Rev. Lett.* **72** 2251 (1994)
8. Landman U et al. *Phys. Rev. Lett.* **77** 1362 (1996)
9. Kondo Y, Takayanagi K *Phys. Rev. Lett.* **79** 3455 (1997)
10. Brandbyge M et al. *Phys. Rev. B* **52** 8499 (1995)
11. Rubio G, Agraït N, Vieira S *Phys. Rev. Lett.* **76** 2302 (1996)
12. Yanson A I et al. *Nature* **395** 783 (1998)
13. Costa-Krämer J L et al. *Surf. Sci.* **342** L1144 (1995)
14. Yanson A I, Yanson I K, van Ruitenbeek J M *Phys. Rev. Lett.* **84** 5832 (2000)
15. Agraït N, Yeyati A L, van Ruitenbeek J M *Phys. Rep.* **377** 81 (2003)
16. Rodrigues V, Fuhrer T, Ugarte D *Phys. Rev. Lett.* **85** 4124 (2000)
17. Kizuka T et al. *Phys. Rev. B* **55** R7398 (1997)
18. Kondo Y, Takayanagi K *Science* **289** 606 (2000)
19. Lagos M J et al. *Nature Nanotechnol.* **4** 149 (2009)
20. Marszalek P E et al. *Proc. Natl. Acad. Sci. USA* **97** 6282 (2000)
21. Kizuka T, Monna K *Phys. Rev. B* **80** 205406 (2009)
22. Sato F et al. *Appl. Phys. A* **81** 1527 (2005)
23. Klavsyuk A L et al. *Eur. Phys. J. B* **85** 331 (2012)
24. Pu Q et al. *J. Chem. Phys.* **126** 144707 (2007)
25. Rubio-Bollinger G et al. *Phys. Rev. Lett.* **87** 026101 (2001)
26. Dreher M et al. *Phys. Rev. B* **72** 075435 (2005)
27. Klavsyuk A L et al. *JETP Lett.* **91** 158 (2010); *Pis'ma Zh. Eksp. Teor. Fiz.* **91** 169 (2010)
28. Liu Y et al. *Phys. Chem. Chem. Phys.* **11** 6514 (2009)
29. Kolesnikov S V, Klavsyuk A L, Saletsky A M *Phys. Solid State* **55** 1950 (2013); *Fiz. Tverd. Tela* **66** 1834 (2013)
30. Kolesnikov S V et al. *Europhys. Lett.* **103** 48002 (2013)
31. Kizuka T *Phys. Rev. B* **77** 155401 (2008)
32. Rodrigues V et al. *Phys. Rev. Lett.* **99** 255501 (2007)
33. Rodrigues V et al. *Phys. Rev. Lett.* **91** 096801 (2003)
34. González J C et al. *Phys. Rev. Lett.* **93** 126103 (2004)
35. Sato F et al. *Phys. Rev. B* **74** 193401 (2006)
36. Takayuki O, Tokushi K *J. Nanosci. Nanotechnol.* **15** 5180 (2015)
37. Rodrigues V et al. *Phys. Rev. B* **65** 153402 (2002)
38. Lagos M J et al. *Nanotechnology* **21** 485702 (2010)
39. Coura P Z et al. *Nano Lett.* **4** 1187 (2004)
40. Cleri F, Rosato V *Phys. Rev. B* **48** 22 (1993)
41. Ercolessi F, Parrinello M, Tosatti E *Philos. Mag. A* **58** 213 (1998)
42. Daw M S, Baskes M I *Phys. Rev. Lett.* **50** 1285 (1983)
43. Jagla E A, Tosatti E *Phys. Rev. B* **64** 205412 (2001)
44. Zhang J-M, Ma F, Xu K-W *Appl. Surf. Sci.* **229** 34 (2004)
45. Tavazza F, Levine L E, Chaka A M *J. Appl. Phys.* **106** 043522 (2009)
46. Koh A S J, Lee H-P *Nano Lett.* **6** 2260 (2006)
47. Klavsyuk A L et al. *Phys. Solid State* **53** 2356 (2011); *Fiz. Tverd. Tela* **53** 2237 (2011)
48. Gülseren O, Ercolessi F, Tosatti E *Phys. Rev. Lett.* **80** 3775 (1998)
49. Bahn S R, Jacobsen K W *Phys. Rev. Lett.* **87** 266101 (2001)
50. Smit R H M et al. *Phys. Rev. Lett.* **87** 266102 (2001)
51. Barzilai S, Tavazza F, Levine L E *J. Phys. Condens. Matter* **25** 325303 (2013)
52. Thijssen W H A et al. *Phys. Rev. Lett.* **96** 026806 (2006)
53. Tsysar K M et al. *Phys. Solid State* **52** 641 (2010); *Fiz. Tverd. Tela* **52** 593 (2010)

54. Qi Y et al. *Phys. Rev. Lett.* **97** 256101 (2006)
55. Smelova K M et al. *Phys. Rev. B* **77** 033408 (2008)
56. Villarreal M A, Oviedo O A, Leiva E P M *J. Chem. Theory Comput.* **8** 1744 (2012)
57. Nakazumi T, Wada Y, Kiguchi M *Nanotechnology* **23** 405702 (2012)
58. Kolesnikov S V, Klavsyuk A L, Saletsky A M *Phys. Rev. B* **80** 245412 (2009)
59. Dokukin S A et al. *Phys. Solid State* **55** 1505 (2013); *Fiz. Tverd. Tela* **55** 1403 (2013)
60. Kolesnikov S V, Klavsyuk A L, Saletsky A M *JETP Lett.* **89** 471 (2009); *Pis'ma Zh. Eksp. Teor. Fiz.* **89** 560 (2009)
61. Oshima Y, Kurui Y *Phys. Rev. B* **87** 081404(R) (2013)
62. Ataca C et al. *Phys. Rev. B* **77** 214413 (2008)
63. Tung J C, Guo G Y *Phys. Rev. B* **81** 094422 (2010)
64. Tsysar K M et al. *JETP Lett.* **94** 228 (2011); *Pis'ma Zh. Eksp. Teor. Fiz.* **94** 246 (2011)
65. Sánchez-Portal D et al. *Phys. Rev. Lett.* **83** 3884 (1999)
66. Bahn S R et al. *Phys. Rev. B* **66** 081405(R) (2002)
67. Legoas S B et al. *Phys. Rev. Lett.* **88** 076105 (2002)
68. Hasmy A et al. *Phys. Rev. B* **78** 115409 (2008)
69. Rodrigues V, Ugarte D *Phys. Rev. B* **63** 073405 (2001)
70. da Silva E Z, da Silva A J R, Fazzio A *Phys. Rev. Lett.* **87** 256102 (2001)
71. Smit R H M et al. *Phys. Rev. Lett.* **91** 076805 (2003)
72. Okamoto M, Takayanagi K *Phys. Rev. B* **60** 7808 (1999)
73. Smelova E M et al. *Moscow Univ. Phys. Bull.* **68** 92 (2013); *Vestn. MGU Ser. 3. Fiz. Astron.* (1) 88 (2013)
74. Fernández-Rossier J et al. *Phys. Rev. B* **72** 224418 (2005)
75. Yu W, Madhukar A *Phys. Rev. Lett.* **79** 905 (1997)
76. Stepanyuk V S et al. *Phys. Rev. B* **69** 033302 (2004)
77. Masuda H, Kizuka T *Jpn. J. Appl. Phys.* **49** 045202 (2010)
78. Deb Nath S K, Kim S-G *J. Appl. Phys.* **112** 123522 (2012)
79. Mehrez H et al. *Phys. Rev. B* **55** R1981 (1997)
80. Lee Y J et al. *Phys. Rev. B* **69** 125409 (2004)
81. Stepanyuk V S et al. *Phys. Rev. B* **72** 153407 (2005)
82. Nilius N, Wallis T M, Ho W *Science* **297** 1853 (2002)
83. Czerner M et al. *Phys. Rev. B* **74** 115108 (2006)
84. Tan Z-Y et al. *J. Appl. Phys.* **114** 063711 (2013)
85. Smelova E M, Tsysar K M, Saletsky A M *Phys. Chem. Chem. Phys.* **16** 8360 (2014)
86. Zheng X et al. *J. Appl. Phys.* **117** 043902 (2015)
87. Landauer R *Philos. Mag.* **21** 863 (1970)
88. Datta S *Quantum Transport: Atom to Transistor* (Cambridge: Univ. Press, 2005); Translated into Russian: *Kvantovyi Transport: ot Atoma k Tranzistoru* (Moscow–Izhevsk: RKhD. Inst. Komp. Issled., 2009)
89. Lesovik G B, Sadovskyy I A *Phys. Usp.* **54** 1007 (2011); *Usp. Fiz. Nauk* **181** 1041 (2011)
90. Todorov T N, Sutton A P *Phys. Rev. B* **54** R14234 (1996)
91. Kurui Y et al. *Phys. Rev. B* **79** 165414 (2009)
92. Pauly F et al. *Phys. Rev. B* **84** 195420 (2011)
93. Tsutsui M, Taniguchi M *J. Appl. Phys.* **113** 024303 (2013)
94. Dremov V V et al. *Phys. Low. Dim. Struct.* **11–12** 29 (1994)
95. Olesen L et al. *Phys. Rev. Lett.* **74** 2147 (1995)
96. Muller C J, van Ruitenbeek J M, de Jongh L J *Phys. Rev. Lett.* **69** 140 (1992)
97. Pascual J I et al. *Phys. Rev. Lett.* **71** 1852 (1993)
98. Klein H et al. *Nanotechnology* **23** 235707 (2012)
99. Untiedt C et al. *Phys. Rev. Lett.* **98** 206801 (2007)
100. Kröger J, Jensen H, Berndt R *New J. Phys.* **9** 153 (2007)
101. Huntington M D et al. *Phys. Rev. B* **78** 035442 (2008)
102. Marchenkov A et al. *Phys. Rev. Lett.* **98** 046802 (2007)
103. García-Suárez V M et al. *Phys. Rev. Lett.* **95** 256804 (2005)
104. Nielsen S K et al. *Phys. Rev. B* **67** 245411 (2003)
105. Dremov V V, Shapoval S Yu *JETP Lett.* **61** 336 (1995); *Pis'ma Zh. Eksp. Teor. Fiz.* **61** 321 (1995)
106. Untiedt C et al. *Phys. Rev. B* **69** 081401(R) (2004)
107. Díaz M, González A C *Physica B* **423** 45 (2013)
108. Jelínek P et al. *Phys. Rev. Lett.* **96** 046803 (2006)
109. Pascual J I et al. *Science* **267** 1793 (1995)
110. Barnett R N et al. *Nano Lett.* **4** 1845 (2004)
111. da Silva E Z et al. *Nanoscale Res. Lett.* **1** 91 (2006)
112. Sclauzero G, Dal Corso A, Smogunov A *Phys. Rev. B* **85** 165412 (2012)
113. Shelykh I A et al. *Semiconductors* **36** 65 (2002); *Fiz. Tekh. Poluprovod.* **36** 70 (2002)
114. Sablikov V A *Semiconductors* **47** 1465 (2013); *Fiz. Tekh. Poluprovod.* **44** 1476 (2013)
115. Velev J et al. *Phys. Rev. Lett.* **94** 127203 (2005)
116. Sokolov A et al. *Nature Nanotechnol.* **2** 171 (2007)
117. Lieb E, Mattis D *Phys. Rev.* **125** 164 (1962)
118. Tung J C, Guo G Y *Phys. Rev. B* **83** 144403 (2011)
119. Sargolzaei M, Ataee S S *J. Phys. Condens. Matter* **23** 125301 (2011)
120. Singh P, Nautiyal T, Auluck S *J. Appl. Phys.* **111** 093506 (2012)
121. Delin A, Tosatti E *J. Phys. Condens. Matter* **16** 8061 (2004)
122. Tung J C, Guo G Y *Phys. Rev. B* **76** 094413 (2007)
123. Klavsyuk A L, Kolesnikov S V, Saletsky A M *JETP Lett.* **99** 646 (2014); *Pis'ma Zh. Eksp. Teor. Fiz.* **99** 759 (2014)
124. Lehnert A et al. *Phys. Rev. B* **82** 094409 (2010)
125. Tsysar K M et al. *Appl. Phys. Lett.* **101** 043108 (2012)
126. Stepanyuk V S et al. *Phys. Rev. B* **70** 195420 (2004)
127. Moseler M et al. *Phys. Rev. Lett.* **86** 2545 (2001)
128. Shinohara T, Sato T, Taniyama T *Phys. Rev. Lett.* **91** 197201 (2003)
129. Delin A, Tosatti E, Weht R *Phys. Rev. Lett.* **92** 057201 (2004)
130. Alexandre S S et al. *Phys. Rev. Lett.* **96** 079701 (2006)